PERSPECTIVE

Check for updates

Modeling heterojunctions: a computational chemistry perspective

Mesfin Eshete and Giovanni Di Liberto (iD) *

The design of heterojunction photocatalysts with enhanced photocatalytic performance is a key challenge. Computational chemistry is a valid strategy to access, with atomistic details, the nature of heterojunction-based materials. In this review, we revise and recall a series of important modeling aspects to account for in the modeling of heterojunctions, such as structural models (including lattice mismatch), band offsets, and interface polarization. Lattice mismatch is essential to be considered to avoid spurious effects. Band offsets determine the relative positioning of the band edges, which in turn indicates the way photogenerated charge carriers prefer to move. The charge polarization has an effect on efficient charge separation which instructs the unidirectional charge migration through the preferential migration path of photogenerated charge carriers. In general, we describe general concepts for designing heterojunction photocatalysts. Drawbacks and potential prospects are discussed to help the field in creating more effective photocatalysts.

1. Introduction

The need for overcoming or at least taming the need for fossil fuels has attracted a lot of attention.[1–3] A possible way to contribute to solving this problem is the use of solar light to make reactions with photocatalysts.[4–7] Investigating highly efficient and environmentally benign photocatalytic materials to convert water into hydrogen is promising for the creation of renewable energy and environmental cleanup.[8–10] In order to accomplish this, current research has focused on

Dipartimento di Scienza dei Materiali, Università degli Studi di Milano Bicocca, Via R. Cozzi 55, 20125 Milano, Italy. E-mail: giovanni.diliberto@unimib.it

thoroughly examining semiconductor photocatalysts with low cost, appropriate band gaps, and high durability to enhance the efficiency of solar-to-hydrogen energy conversion.[11–13]

Semiconductor photocatalysis is a promising and environmentally favorable technology.[14–17] During excitation by UV or visible light, electrons are promoted from the valence band maximum (VBM) to the conduction band minimum (CBM), leaving holes in the valence band. The two photo-generated charge carriers can in principle promote reactions of interest. Several different oxides are used, such as TiO_2,[4,18] ZnO,[19,20] Cu_2O,[21,22] and others.[23,24] However, these materials often suffer from performance limitations due to two drawbacks: high band gap and fast charge carrier

Mesfin Eshete

Mesfin Eshete is a research fellow at the Department of Materials Science, University of Milano Bicocca. He received his Ph.D. from the University of Science and Technology of China in 2020. His main research interests are structural and electronic properties of novel materials, electron dynamics at the surface and interface, and design of novel heterojunctions in energy conversion for application of photocatalysis, catalysis, perovskites and single-atom catalysis.

Giovanni Di Liberto

Giovanni Di Liberto received the PhD in Chemistry in 2019. He is a tenure-track assistant professor at the Department of Materials Science, University of Milano Bicocca, Italy. His research is devoted to the simulations of nanomaterials for catalysis. He was a visiting scientist at the University of Barcelona in 2019. He has obtained awards from the physical chemistry, theoretical and computational chemistry and catalysis divisions of the Italian Chemical Society over the past few years.

© 2025 The Author(s). Published by the Royal Society of Chemistry

RSC Appl. Interfaces, 2025, **2**, 897–916 | 897

recombination. The fabrication of heterojunctions has been suggested to tame the limitations of single-phase semiconductors.[25–28] In heterojunctions, it is possible to improve the separation of charge carriers by engineering the alignment of the band edges. Also, one component of the system can act as a sensitizer improving the absorption of visible light.[14,29–31]

Increased rates of charge migration and separation, and the use of a broad spectrum of solar light, lead to the improved photocatalytic efficiency of these devices. Key examples in this regard are TiO_2/TiO_2 and $TiO_2/BiVO_4$ junctions.[32,33]

Over the past ten years, numerous photocatalysts have been created and applied to a variety of reactions, including water splitting, wastewater treatment, and CO_2 reduction.[9,11,26,34] To deeply analyze the charge dynamics and mechanism of a heterojunction, one needs to focus on the materials synthesis and characterization techniques and also theoretical modeling.[12,13,23] Recently, many techniques have been employed to boost the performance of photocatalytic materials, including doping, nanostructuring, semiconductor heterojunction formation, co-catalyst use, or a mix of these methods.[9,12,31,35] For example, the formation of a metal–semiconductor Schottky junction can help the electron–hole separation, while the plasmonic effect of noble metals has been used to increase the light absorption of wide-band gap semiconductors.[23,36,37] In general, design of heterojunction photocatalysts must consider: (1) appropriate band edge positioning of the VB and CB, (2) efficient charge separation of photoexcited electron–hole pairs upon light illumination and (3) chemical stability.[15,34,38–40]

In principle, heterojunctions can be classified as p–n junctions (type-I, type-II and type-III), Fig. 2, Z-scheme (including S-scheme), Fig. 3, and ternary heterojunctions, Fig. 4. In this context, the ability to create and design interfaces between various semiconductors allow a wide range of systems to be investigated. In such investigation, consideration of lattice mismatch with the two or more interface structures, the charge transfer mechanism, interface polarization, the nature of chemical bonds, the band gap and band edge positions are important aspects. Density functional theory (DFT)-based electronic structure computations are crucial in this setting.

The number of applications of heterojunctions is very vast, ranging from energy to environmental remediation. The potential of these systems has stimulated increasing interest, which can be clearly shown by scrutinizing the number of publications related to the field, Fig. 1a. Nowadays, thousands of publications are reported every year, related to CO_2 reduction, water splitting, hydrogen generation and photodegradation of pollutants, Fig. 1b.

Quantum chemical calculations allow us to provide atomistic insight into the nature of heterojunction materials. The state-of-the-art approach is based on density functional theory (DFT). This tutorial review focuses on the designs with quantum chemical approaches for different semiconductor heterojunctions. In addition, a detailed emphasis is given to
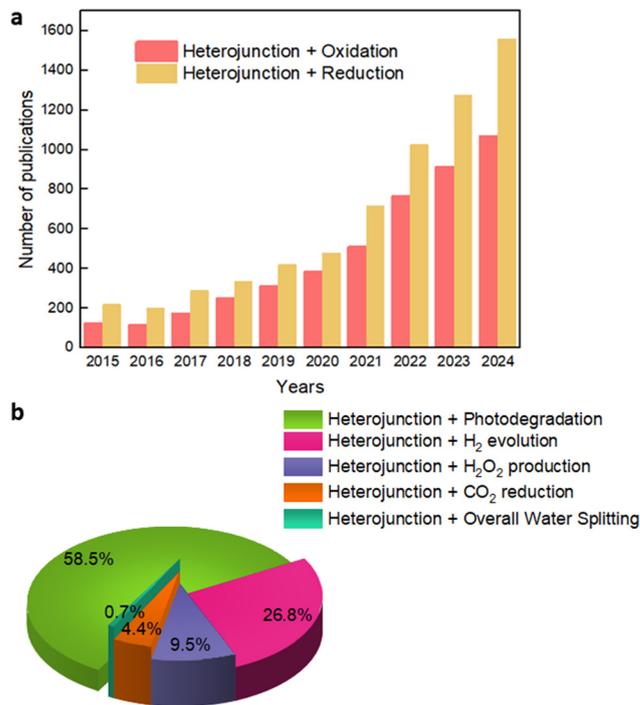

Fig. 1 (a) Bar graph presentation from Scopus on the number of publications from 2015 to 2024, using keywords "heterojunction + oxidation" and "heterojunction + reduction". (b) Pie chart on the adopted keywords.

structural and electronic properties at the interface including the band edge position, band edge offsets, built-in electric field and charge polarization at the interface.

2. Different types of heterojunctions

2.1. Semiconductor–semiconductor (S–S) heterojunctions

Heterostructures are typically classified according to the relative alignment of the band edges. One can then refer to type I, type II, and type III heterostructures, Fig. 2. In the type-I junction, the valence band maximum (VBM) and conduction band minimum (CBM) of one component are within the band gap of the second unit composing the system, Fig. 2a. Photogenerated charge carriers will migrate (thermodynamically) toward the first phase. In a type-II junction, the band edges of one component are higher in energy than the second, Fig. 2b. If the VBM of one component is higher in energy than the CBM of the second unit, then a type-III junction is formed, Fig. 2c. In this type, photoinduced charges lose their energy while traveling long distance to reach their neighbor CB/VB. In type I (straddling band gap), high energy electrons and holes transfer to the same semiconductor, preventing photocatalytic activity.[41,42] The type-II system is the ideal one for charge carrier separation, as photogenerated holes and electrons will be promoted to spatially separate in the different phases. In addition, the efficiency can also be enhanced by forming ternary heterojunction catalysts by
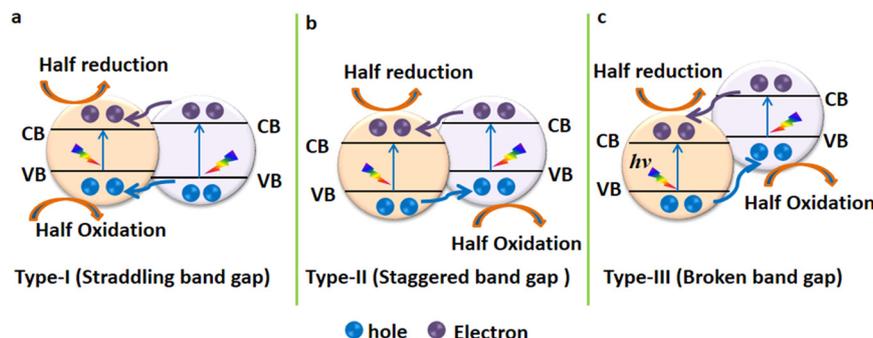
Fig. 2 Schematic diagrams of type I (panel a), II (panel b) and III (panel c) junctions.

integrating type II heterostructures with noble metals.[43,44] Table 1 lists a series of possible type-II heterojunctions and their applications.

The photocatalytic performance of S–S heterojunctions is limited by some drawbacks, even though better charge separation and enhanced photocatalysis are achieved. In particular, the charge carrier migration is accompanied by a partial loss of energy of the absorbed photons, which lowers the photocatalytic activity.

2.2. Z-scheme heterojunctions

Even though better charge separation is achieved in p–n heterojunctions, most of them fall to straddling band gaps (type I) (Fig. 2a). In such cases, both photogenerated electrons and holes migrate to the narrow band gap semiconductor, which leads to a high rate of recombination. On the other hand, type-II and type-III (Fig. 2b and c) junctions guarantee efficient charge separation onto distinct semiconductors.

In recent years, more complex systems have been proposed. Relevant examples are the so-called Z-scheme junctions. The Z-scheme combines two distinct photocatalysts with the help of a suitable shuttle redox couple, such as Fe^{3+}/Fe^{2+} and IO_3^-/I^-. Compared to conventional one-step water splitting systems, visible light can be used more efficiently.[79–82]

Z-scheme heterostructures are depicted in Fig. 3a, where the three elements composing the system are reported, the two photocatalysts and redox couple in aqueous solution.

Table 1 A summary of available experimental examples of heterojunctions

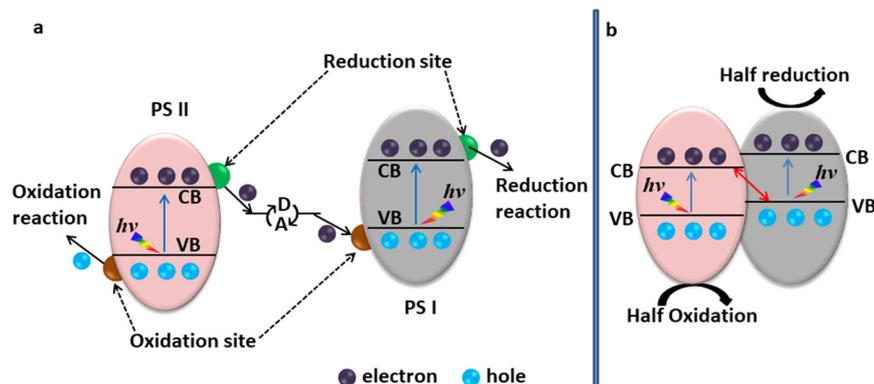| Model	Type	Application	References
CdS/Cu_2O	Type II	H_2 generation	45
$\alpha\text{-}Fe_2O_3/ZnO$	Type II	H_2 production	46
$TiO_2/BiOBr$	Type II	Degradation of rhodamine B (RhB) and methyl orange (MO)	47
$BaTiO_3/CuO$	Type I	MO degradation	48
ZnO/NiO	Type II	Degradation of RhB	49, 50
SnO_2/NiO	Type II	Degradation of RhB	51
$CuCo_2O_4/TiO_2$	Type II	H_2 evolution	52
MoS_2/WSe_2	Type II	H_2 production	53, 54
TiO_2/Cu_2O	Type II	H_2 generation	55–58
$Cu_3SnS_4/BiVO_4$	Type II	Degradation of methyl blue (MB)	59
MoS_2/TiO_2	Type II	H_2 generation, degradation of MB and acetone	60
CdS/CuS	Type II	H_2 production	61
$BiFeO_3/ZnO$	Type II	Photodegradation of 2,4-dichlorophenol and RhB	62
ZnO/TiO_2	Type II	H_2 production	63
$BiOBr/BiVO_4$	Type II	Degradation of MB	64
$\alpha\text{-}Fe_2O_3/CuPc$	Type II	Photoreduction of CO_2	65
SnO_2/Bi_2O_3	Type II	Degradation of RhB	66
$Ag_3PO_4/AgBr$	Type II	Degradation of MB	67
$CdS/LaFeO_3$	Type II	Degradation of MB, RhB, and MO	68
CoP_3/Ni_2P	Type II	H_2 production	69
ZnO/CuO	Type II	Photodegradation of phenol	70, 71
CuO/TiO_2	Type II	Degradation of MB	72
TiO_2/CeO_2	Type II	Oxidative degradation of crystal violet (CV)	73
TiO_2/CuS	Type II	H_2 generation	74
Fe_2O_3/Co_3O_4	Type II	Overall water splitting	75
WO_3/MoS_2	Type II	Degradation of Congo red (CR)	76
SnO_2/CuO	Type II	Decomposition of MB	77
ZnO/SnS	Type II	Degradation of MO and RhB	78

Fig. 3 a) Schematic representation of the Z-scheme. b) Schematic representation of the S-scheme.

When a photocatalyst (PS II) is photoexcited, the excited electrons migrate from the lower CB to the redox couple, which in turn transfers the electrons to the other semiconductor (PS I) and the electrons recombine with the holes formed at the VBM of PS I. As a result, holes will concentrate at the photocatalyst with a lower VBM, whereas electrons will accumulate on the photocatalyst with a higher CBM. This strategy allows increasing the redox power of the charge carriers.[38,40,83] An alternative solution is to replace the redox couple with a metal.[34,79,84,85] A list of Z-scheme heterojunctions reported in the literature is in Table 2.

The efficiency of Z-schemes is highly dependent on the locations to the band positions of the VB of semiconductor 1 and the CB of semiconductor 2 relative to the redox potential of the AD species. This limits the combinations of semiconductors that can produce effective photocatalytic heterojunctions. Another possible approach is S-scheme heterojunctions, without a shuttle redox mediator as discussed here after.

2.3. S-scheme heterojunctions

A very special case of Z-scheme systems are the S-scheme junctions, Fig. 3b. In an S-scheme heterojunction, a critical role is played by the interface polarization. Indeed, if an interface dipole is generated with an appropriate orientation, it is possible to promote the spatial separation of charge carriers opposite to what happens to classical type-II systems. As a result, high energy electrons and holes separate in different semiconductors.[39,40,108,109] Table 3 summarizes a few S-scheme heterojunctions applied in the literature.

2.4. Ternary heterojunctions

The discussion was limited to two-phase systems. Nowadays, it is possible to invoke more involved catalytic systems made by three (or more) components. In ternary heterojunction photocatalysts, three semiconductors can be combined to create direct Z-schemes. These photocatalysts are commonly referred to as "ternary Z-schemes" or "dual Z-schemes".

Table 2 A summary of available experimental examples of Z-scheme heterojunctions

Model	Type	Application	References
$Fe_2O_3/ZnSe$	Z-scheme	CO_2 to CO photoconversion	86
$BiVO_4/Cu_2O$	Z-scheme	CO_2 reduction	87, 88
$CsPbBr_3/BiOC$	Z-scheme	CO_2 reduction	89
$ZnIn_2S_4/BiPO_4$	Z-scheme	Cr(VI) removal	90
$BiOBr/Bi_2WO_6$	Z-scheme	Degradation of tetracycline (TC)	91
$ZnIn_2S_4/TiO_2$	Z-scheme	Overall water splitting	92
TiO_2/NiO	Z-scheme	H_2 evolution	93
$Ag_2O/Fe–TiO_2$	Z-scheme	CO_2 conversion into methane	94
$NiSe_2/Co-CdS$	Z-scheme	H_2 evolution	95
$ZnO/Ag/Ag_2WO_4$	Z-scheme	Photoelectrochemical water oxidation	96
$Bi_2WO_6/Au/CdS$	Z-scheme	CO_2 reduction	97
$TiO_2/Au/g-C_3N_4$	Z-scheme	CO_2 reduction	98
$g-C_3N_4/Au/ZnO$	Z-scheme	CO_2 reduction	36
$g-C_3N_4/Au/SnS$	Z-scheme	CO_2 reduction	99
$Ag_3PO_4/Ag/GdCrO_3$	Z-scheme	CO_2 reduction	100
$BiVO_4(010)/Au/Cu_2O$	Z-scheme	CO_2 reduction	101
$WO_3/Ag/GdCrO_3$	Z-scheme	Photothermocatalytic toluene degradation and CO_2 reduction	102
$TiO_2/Cu/CaTiO_3$	Z-scheme	H_2 evolution	103
$g-C_3N_4/WO_3/Ag$	Z-scheme	Degradation of oxytetracycline hydrochloride	104
$BiOBr/Ag_3PO_4/Rgo$	Z-scheme	Degradation of TC	105
$SnS_2/RGO/g-C_3N_4$	Z-scheme	Degradation of organic dye	106
$SnS_2/LaNiO_3$	Z-scheme	Degradation of TC	107

Table 3 A summary of available experimental examples of S-scheme heterojunctions

Model	Type	Application	References
ZnCdS/ZnS	S-scheme	H_2 evolution	110
CdS/Mo$_2$C	S-scheme	H_2 evolution	111
α-Fe$_2$O$_3$/CeO$_2$	S-scheme	H_2 evolution	112
α-Fe$_2$O$_3$/TiO$_2$	S-scheme	H_2 evolution	113
ZnIn$_2$S$_4$/NiTiO$_3$	S-scheme	H_2 evolution	114, 115
TiO$_2$/ZnIn$_2$S$_4$	S-scheme	H_2 evolution	116–118
ZnIn$_2$S$_4$/ZnWO$_4$	S-scheme	H_2 evolution	119
WO$_3$/BiOBr	S-scheme	Degradation of TC and enrofloxacin (ENR)	120
BiOI/TiO$_2$	S-scheme	Degradation of RhB	121
Bi$_3$TaO$_7$/ZnIn$_2$S$_4$	S-scheme	H_2 evolution	122
Co$_9$S$_8$/In$_2$O$_3$	S-scheme	H_2 evolution	123
Co$_9$S$_8$/Bi$_2$S$_3$	S-scheme	H_2 evolution	124
CdS/BiOIO$_3$	S-scheme	CO_2 reduction	125
Co$_3$Se$_4$/TiO$_2$	S-scheme	H_2 evolution	126
BiVO$_4$/CeO$_2$	S-scheme	CO_2 reduction	127
TiO$_2$/CdS	S-scheme	Overall water splitting	128
ZnIn$_2$S$_4$/CdIn$_2$S$_4$	S-scheme	CO_2 reduction	129
Cs$_2$AgBiBr$_6$/Bi$_2$WO$_6$	S-scheme	CO_2 reduction	130
CsPbBr$_3$/AgBr	S-scheme	CO_2 reduction	131
In$_4$SnS$_8$/Cs$_3$Bi$_2$Br$_9$	S-scheme	Photoreduction CO_2 and CO selectivity	132
ZnO/WO$_3$	S-scheme	H_2O_2 production	133
WO$_3$/ZnIn$_2$S$_4$	S-scheme	H_2 production	134
MoS$_2$/BiVO$_4$	S-scheme	Degradation of RhB	135
BiVO$_4$/Ag$_3$VO$_4$	S-scheme	Degradation of MB	136
Bi$_2$S$_3$/CeVO$_4$	S-scheme	Degradation for naphthalene (NAP)	137
Cu$_{2-x}$S/TiO$_2$	S-scheme	CH_4 production	138
MoS$_2$/2D PbTiO$_3$	S-scheme	Degradation of MB	139
MoS$_2$/Ag$_3$PO$_4$	S-scheme	Removal of RhB and ofloxacin (OFL)	140
Bi$_2$WO$_6$/Bi$_2$O$_3$	S-scheme	H_2 production	141
BiVO$_4$/CsPbBr$_3$	S-scheme	CO_2-to-CO conversion	142
NiS$_2$/MoSe$_2$	S-scheme	H_2 evolution	143
LaNiO$_3$/TiO$_2$	S-scheme	Degradation of MO	144
CeO$_2$/ZnIn$_2$S$_4$	S-scheme	H_2 production	145
In$_2$S$_3$/Bi$_2$O$_2$CO$_3$	S-scheme	Degradation of RhB and TC	146
Cu$_3$SnS$_4$/L-BiOBr	S-scheme	Ciprofloxacin degradation	147
TiO$_2$/FePS$_3$	S-scheme	H_2 production	148
BiOBr/Bi$_2$WO$_6$	S-scheme	CO_2 reduction	149
ZnIn$_2$S$_4$/WO$_3$	S-scheme	H_2 production	150
FeS$_2$/ZnIn$_2$S$_4$	S-scheme	H_2 production	151
AgBr/BiOBr	S-scheme	CO_2 reduction and H_2 production	152
FeS$_2$/S-ZnSnO$_3$	S-scheme	H_2 evolution	153
Bi$_2$O$_2$S/NiFe$_2$O$_4$	S-scheme	Degradation of TC	154
Bi$_2$MoO$_6$/BiOI	S-scheme	CO_2 reduction	155
BiFeO$_3$/Bi$_2$Fe$_4$O$_9$	S-scheme	O-chlorophenol degradation	156
CuWO$_{4-x}$/Bi$_{12}$O$_{17}$Cl$_2$	S-scheme	Degradation of TC	157
Cu2O/ BiOI	S-scheme	CO_2 reduction	158
In$_2$O$_3$/ZnO	S-scheme	CO_2 reduction	159
Ta$_3$N$_5$/BiOCl	S-scheme	Degradation of TC and Cr(VI)	160
WO$_3$/TiO$_2$	S-scheme	H_2 production	161
NiCo$_2$S$_4$/ZnIn$_2$S$_4$	S-scheme	H_2 production	162
Co$_9$S$_8$/ZnSe	S-scheme	H_2 production	163
SnO$_2$/SnS$_2$	S-scheme	Overall water splitting	164
WO$_3$/CuBi$_2$O$_4$	S-scheme	CO_2 reduction	165
BaTiO$_3$/TiO$_2$	S-scheme	Norfloxacin degradation	166
WS$_2$/BiYWO$_6$	S-scheme	Degradation of RhB	167
Bi$_{12}$O$_{17}$Cl$_2$/α-Bi$_2$O$_3$	S-scheme	Degradation of TC	168
BiOCl/MoS$_2$	S-scheme	Degradation of TC	169
Ag$_3$CuS$_2$/VO$_2$	S-scheme	MB photodegradation and Cr(VI) photocatalytic reduction	170
ZnS/CoMoO$_4$	S-scheme	H_2 production	171
CuCo$_2$O$_4$/CeO$_2$	S-scheme	CO_2 reduction	172
SnFe$_2$O$_4$/ZnFe$_2$O$_4$	S-scheme	Degradation of TC	173
Bi$_2$Sn$_2$O$_7$/Bi$_2$MoO$_6$	S-scheme	Degradation of TC	174

These systems promote spatial separation of electron–hole pairs, which favors reduction and oxidation reactions. In addition, it is possible to increase the absorption of visible light.[35,38,175,176] A schematic representation of the alignment
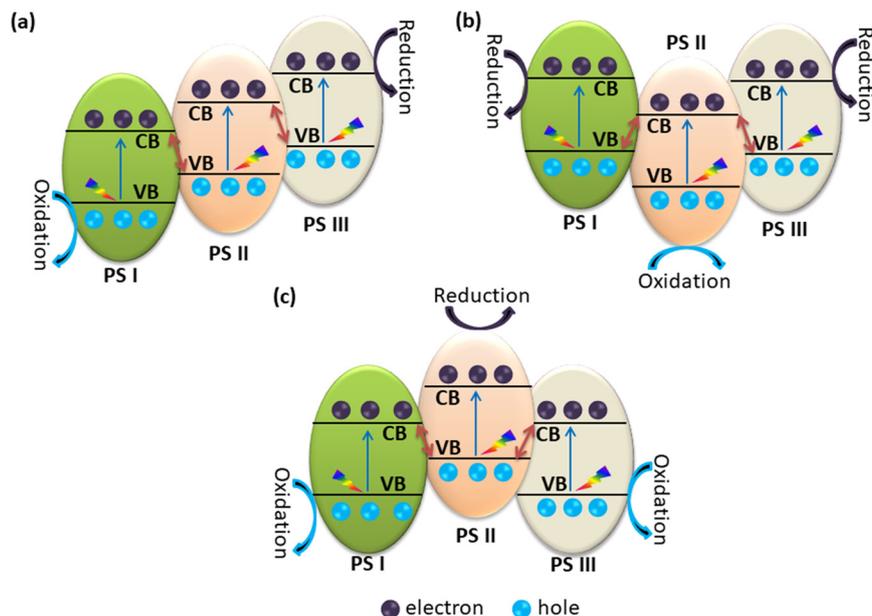
Fig. 4 Systematic representation of ternary heterojunctions. (a) Cascade type ternary heterojunction. (b) Arrow-down type ternary heterojunction. (c) Arrow-up type heterojunction.

of the band edges of ternary heterojunctions is reported in Fig. 4. Typically, ternary heterojunctions are categorized as cascade-type (Fig. 4a), arrow-up (Fig. 4b) and arrow-down (Fig. 4c) Z-scheme systems.[35]

In the case of the cascade Z-scheme, the excited electrons will concentrate toward the system with the highest CBM. At the same time, holes will follow an opposite path, concentrating to the system with the lowest VBM, Fig. 4a. In an arrow-down system, the holes in PS I and PS III's VBs join with the electrons in PS II's CB, as depicted Fig. 4b. In this ternary Z-scheme, the excited electrons from PS II combine with the holes in both PS III and PS I, thus favoring the oxidation on semiconductor PS II and reduction on PS III and PS I. The other type is an arrow-up Z-scheme ternary heterojunction. In this heterojunction, the excited electrons from the CB of PS I and PS III migrate and combine with the holes at the VB of PS II. Consequently, oxidation can take place on PS III and PS I while reduction on PS II, as depicted in Fig. 4c. A summary of typical ternary heterojunctions is reported in Table 4.

2.5. 2D/2D heterojunctions

It has been shown that ultrathin 2D materials have special physical, chemical, and electronic properties. These properties include high carrier mobility, large specific surface area and unique optical band gaps.[212–215]

Two-dimensional (2D) heterojunctions have benefits for catalysis because of their large surface area, ultrathin thickness and short charge migration distance across the interface. In general, 2D interfaces maximize quantum efficiency, broadening the range of light absorption for improved photocatalytic activity compared to three-dimensional interfaces. Consequently, the creation and application of 2D/2D heterojunctions has quickly emerged as one of the most popular areas of study.[216–222]

It is possible to generate 2D/2D heterostructures using various contact interfaces oriented laterally or vertically as depicted in Fig. 5. By stacking two or more monolayers of various materials in a vertical direction, 2D/2D heterostructures with a face-to-face interface contact can be created, Fig. 5a and b. Alternatively, both paralleled and patterned connections, like the heterostructures in Fig. 5c and d, can be created in a lateral direction.[223–226] A special case in the family of 2D-based heterojunctions is carbon nitride. Carbon nitride is one of the most promising metal-free photocatalysts for efficient utilization of sunlight. A comprehensive summary of typical g-C$_3$N$_4$ heterojunctions is shown in Table 5.
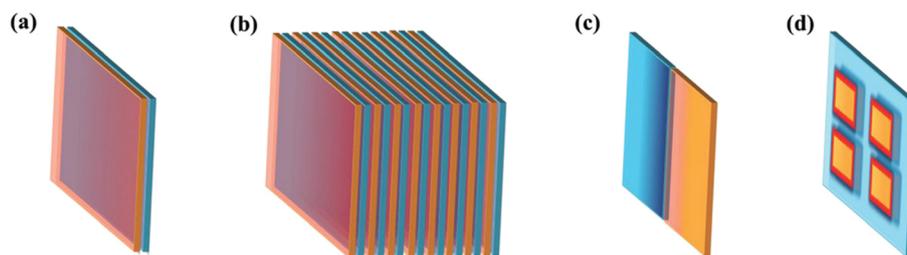
3. How to model an interface

3.1. Importance of structural engineering

The design of suitable interface models is a crucial step in the construction of heterojunctions. When modeling an interface, one needs to accommodate two different material surfaces in the same simulation cell. This introduces an unavoidable lattice mismatch, i.e. the lattice parameters of the interface do not correspond exactly to those of the independent units. Ideally, a well-designed interface should have the smallest possible lattice mismatch. Importantly, the electronic structure of the heterostructure is affected by the strain at the interface that resulted from the lattice mismatch.[23,26,295] A good practice always consists of a checking post-process, i.e. after geometry optimization of the interface model that

Table 4 A summary of available experimental examples of ternary heterojunctions

Model	Type	Application	References
$TiO_2/Ti_3C_2/g\text{-}C_3N_4$	Cascade	H_2 production	177
$Cu_2O/ZnO/Ag_3PO_4$	Arrow-up	Degradation of MO	178
$ZnS/ZnO/g\text{-}C_3N_4$	Cascade	H_2 production	179
$Bi_2S_3/MoS_2/TiO_2$	Cascade	Degradation of MB and CO_2 reduction	180, 181
$ZnO/CuO/CeO_2$	Arrow-down	Degradation of CV and MO	182
$g\text{-}C_3N_4/ZnO/CeO_2$	Cascade	Degradation of MB	183
$WO_3/g\text{-}C_3N_4/WS_2$	Arrow-up	Degradation of RhB and MO	184
$Bi_2O_3/CeO_2/ZnO$	Arrow-up	Degradation of RhB	185
$ZnO/NiWO_4/Ag_2CrO_4$	Arrow-down	Degradation of MB, MO, and fuchsine	186
$ZnO/Bi_2MoO_6/AgBr$	Arrow-up	Degradation of RhB	187
$ZnO/CoWO_4/Ag_3VO_4$	Arrow-down	Degradation of RhB	188
$O\text{–}g\text{-}C_3N_4/Zn_2SnO_4N/ZnO$	Cascade	Degradation of organic dyes and NO removal	189
$ZnO/ZnS/g\text{-}C_3N_4$	Cascade	H_2 production	190
$ZnFe_2O_4/ZnO/CdS$	Cascade	CO_2 reduction	191
$CNT/NCDs/Ni_2P$	Cascade	H_2 production	192
$MoP_4/Ni_3S_2/MoO_3$	Arrow-up	Overall water splitting	193
$g\text{-}C_3N/Bi_2WO_6/AgI$	Arrow-up	Removal of tetracycline	194
$g\text{-}C_3N_4/Bi_4Ti_3O_{12}/Bi_4O_5I_2$	Arrow-up	H_2 production and ofloxacin (OFL) removal	195
$BiOCl/BiVO_4/N\text{-}GQD$	Arrow-up	Photodegradation of bisphenol A	196
$Ag_3PO_4/Co_3(PO_4)_2/g\text{-}C_3N_4$	Arrow-up	Degradation of TC	197
$WSe_2/In_2S_3/ZnIn_2S_4$	Arrow-up	Degradation of MB	198
$TiO_{2-x}/BiOI/AgBr$	Arrow-up	Degradation of RhB	199
$BiOBr/ZnO/BiOI$	Arrow-up	Degradation of RhB	200
$Cu_2O/S\text{-}TiO_2/CuO$	Arrow-down	CO_2 conversion	201
$TiO_2/ZnO/SnO_2$	Cascade	Degradation of 2,4-dichlorophenol (2,4-DCP) and bisphenol A (BPA)	202
$CdS/1\ T\text{-}MoS_2/TiO_2$	Arrow-down	H_2 production	203
$TiO_2/CdS/MoS_2$	Arrow-up	H_2 production	204
$Cu2O/WO3/CeO2$	Cascade	CO_2 reduction	205
$ZnIn_2S_4/Ni_{12}P_5/g\text{-}C_3N_4$	Cascade	CO_2 and H_2O_2 production	206
$g\text{-}C_3N_4/CuFe_2O_4/ZnIn_2S_4$	Cascade	CO_2 reduction	207
$Bi_2S_3/\beta\text{-}Bi_2O_3/ZnIn_2S_4$	Arrow-down	H_2 production and degradation of TC	208
$Ag_2CO_3/Bi_4O_5I_2/g\text{-}C_3N_4$	Arrow-down	Degradation of TC	209
$MoS_2/Bi_2S_3/BiVO_4$	Arrow-up	Degradation of fluoroquinolones	210
$In_2S_3/Nb_2O_5/Nb_2C$	Arrow-up	H_2 production	211

Fig. 5 Methodical representation of 2D/2D heterostructures with various contacts, face-to-face (a and b), lateral and parallel (c and d). Reproduced with permission.[223] Copyright 1999–2025 John Wiley & Sons.

the lattice mismatch of the independent units does not alter their electronic structure, such as the band gap and band edge positioning. Typically, it is considered acceptable if the lattice mismatch induces changes in band edges and the band gap within 0.1 eV. Typically, it is possible to achieve a small lattice mismatch by invoking a rotational angle between the two composing units. For instance, the interface between two stable $BiOIO_3$ surfaces, (010) and (100), can be obtained with a relatively small lattice mismatch, lower than 2% for both a and b lattice parameters with good cation–anion

matching achieved by rotating the two surfaces by 90 degrees. The impact of lattice mismatch is very small, about 0.1 eV.[296,297]

The introduction of lattice mismatch comes from the need for designing an *a priori* suitable working simulation cell for the heterostructure. A better-grounded approach consists of avoiding the need for introducing lattice mismatch. This is possible by invoking unconstrained energy mapping of material interfaces. Among the possible strategies, Fig. 6 reports the case of the "rotating nanodisk" approach. In this framework, disk-shaped nanoparticles of

© 2025 The Author(s). Published by the Royal Society of Chemistry

RSC Appl. Interfaces, 2025, **2**, 897–916 | **903**

Table 5 A summary of available experimental examples of g-C$_3$N$_4$ heterojunctions

Model	Type	Application	References
g-C$_3$N$_4$/WO$_3$	Type II	CO$_2$ reduction, Cr(VI) reduction and MB degradation	227, 228
BiVO$_4$/g-C$_3$N$_4$	Z-scheme	Overall water splitting	229, 230
g-C$_3$N$_4$/BiFeO$_3$	Direct Z-scheme	Overall water splitting	231
g-C$_3$N$_4$/Bi$_2$WO$_6$	Z-scheme	Ciprofloxacin photodegradation	232
α-Fe$_2$O$_3$/g-C$_3$N$_4$	Direct Z-scheme	Overall water splitting	233
g-C$_3$N$_4$/TiO$_2$	Type II	Overall water splitting, degradation of diclofenac	234–236
AgCl/g-C$_3$N$_4$	S-scheme	H$_2$ production	237
MnCo$_2$S$_4$/g-C$_3$N$_4$	S-scheme	H$_2$ production	238
BiOIO$_3$/g-C$_3$N$_4$	Z-scheme	Degradation of NO	239
W$_{18}$O$_{49}$/g-C$_3$N$_4$	Direct Z-scheme/S-scheme	Overall water splitting	240–242
Bi$_4$NbO$_8$Cl/g-C$_3$N$_4$	Direct Z-scheme	H$_2$ evolution	243
Cu$_2$O/g-C$_3$N$_4$	Type II	H$_2$ production	244
K$_4$Nb$_6$O$_{17}$/g-C$_3$N$_4$	Z-scheme	Organic pollutant removal and H$_2$ production	245
Bi$_2$S$_3$/g-C$_3$N$_4$	Z-scheme	Photoreduction of CO$_2$ to CO	246
Ag$_3$PO$_4$/ g-C$_3$N$_4$	S-scheme	O$_2$ production and conversion of Cr(VI) to Cr(III)	247
g-C$_3$N$_4$/Bi$_8$(CrO$_4$)O$_{11}$	S-scheme	Degradation of norfloxacin and BPA	248
CoFe$_2$O$_4$/ g-C$_3$N$_4$	S-scheme	Degradation of TC, amoxicillin, ciprofloxacin, and sulfamethoxazole	249
Bi$_4$V$_2$O$_{11}$/g-C$_3$N$_4$	S-scheme	Photocatalytic antibiotic degradation	250
Fe-g-C$_3$N$_4$/Bi$_2$WO$_6$	Z-scheme	Degradation of TC	251
MnCo$_2$O$_4$/g-C$_3$N$_4$	Type II	H$_2$ production	252
WS$_2$/g-C$_3$N$_4$	Type I	H$_2$ production	253
CuInS$_2$/g-C$_3$N$_4$	Direct Z-scheme	H$_2$ evolution	254
Cu$_3$P/g-C$_3$N$_4$	Type II	H$_2$ evolution	255
LaCoO$_3$/g-C$_3$N$_4$	Z-scheme	Phenol degradation	256
MnIn$_2$S$_4$/g-C$_3$N$_4$	Direct Z-scheme	H$_2$ evolution	257
ZnSe/g-C$_3$N$_4$	Type II	H$_2$ evolution	258
g-C$_3$N$_4$/SnS	Type II	Reduction of aqueous Cr(VI)	259
g-C$_3$N$_4$/Ag$_3$PO$_4$	Z-scheme	Degradation of TC and dye	260
g-C$_3$N$_4$/BiOBr	Type II	Oxidation of NO and reduction of CO$_2$	261
Fe$_2$O$_3$/g-C$_3$N$_4$	Direct Z-scheme	H$_2$ evolution	262
O-g-C$_3$N$_4$/B-RGO	Type II	H$_2$ evolution	263
g-C$_3$N$_4$/Nb$_2$O$_5$	Type II	Degradation of RhB and phenol	264
g-C$_3$N$_4$/C-doped BN	Direct Z-scheme	H$_2$ evolution	265
g-C$_3$N$_4$/MnO$_2$	Z-scheme	Dye degradation and phenol removal, overall water splitting	266, 267
CdS/g-C$_3$N$_4$	Z-scheme	H$_2$ production	268
CoO/g-C$_3$N$_4$	Type II	Evolution of H$_2$ and O$_2$	269
O–C$_3$N$_4$/SnS$_2$	S-scheme	H$_2$ evolution	270
ZnO/g-C$_3$N$_4$	S-scheme	Degradation of MB	271
NiSe$_2$/g-C$_3$N$_4$	Type II	CO$_2$ reduction	272, 273
TiO$_2$/g-C$_3$N$_4$	Z-scheme	Degradation of RhB	274
CoNi$_2$S$_4$/g-C$_3$N$_4$	Type II	Evolution of H$_2$ and O$_2$	275
TiO$_2$/*g*-C$_3$N$_4$	Type II	Degradation of MB, decomposition of fluorescein	276, 277
BiOBr/g-C$_3$N$_4$	S-scheme	Degradation of RhB	278, 279
g-C$_3$N$_4$/Bi$_{12}$O$_{17}$Cl$_2$	S-scheme	CO$_2$ reduction	280
Cu$_2$O/g-C$_3$N$_4$	S-scheme	Oxidation TC, reduction of Cr(VI) and H$_2$ evolution	281
CoWO$_4$/g-C$_3$N$_4$	S-scheme	H$_2$ production	282
Co$_3$O$_4$/ g-C$_3$N$_4$	S-scheme	Degradation of TC	283
NiCo$_2$O$_4$/g-C$_3$N$_4$	S-scheme	H$_2$ production	284
Bi$_3$NbO$_7$/g-C$_3$N$_4$	S-scheme	CO$_2$ reduction	285
g-C$_3$N$_4$/Bi$_2$MoO$_6$	S-scheme	Degradation of phenol and H$_2$ evolution	286
g-C$_3$N$_4$/CoTiO$_3$	S-scheme	H$_2$ production	287
Ni$_5$P$_4$/g-C$_3$N$_4$	S-scheme	H$_2$ production and carbamazepine degradation	288
g-C$_3$N$_4$/Nb$_2$O$_5$	S-scheme	CO$_2$ reduction	289
g-C$_3$N$_4$/MoO$_{3-x}$	S-scheme	H$_2$ evolution	290
WO$_3$/g-C$_3$N$_4$	S-scheme	H$_2$ evolution	291
CdS/g-C$_3$N$_4$	S-scheme	Overall water splitting	292
ZnO/g-C$_3$N$_4$	S-scheme	H$_2$O$_2$ production	293
g-C$_3$N$_4$/TiO$_2$	S-scheme	Degradation of MB and RhB	294

separated units are generated, and they are interfaced by sampling three different degrees of freedom: the in-plane displacement, $s = (s_x, s_y)$, and the rotational angle, α. In this way, it is possible to sample the energy landscape of heterostructures, and if 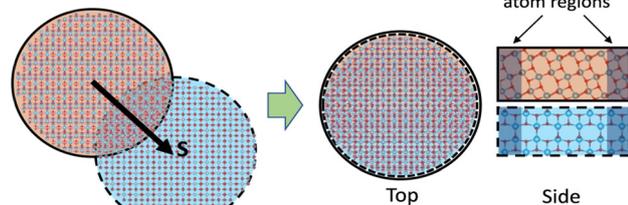the size of the disks is sufficiently large, typically a radius of 2.5 nm is a good trade-off; the effect of lattice mismatch is not sizeable. It must be mentioned that free-fitted potential energy surfaces or force fields are needed to sample the energy landscape, and therefore the resulting structures must be used as starting
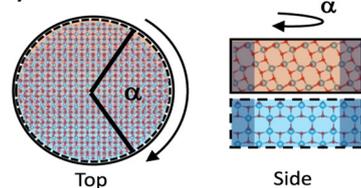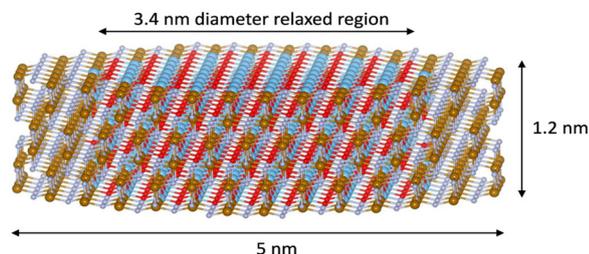
Fig. 6 Systematic approach to exploring disk interface models for the TiO₂ anatase (101)/(001) interface. (a) Two disks are cut from the TiO$_2$ (101) and (001) reference slabs. (b) The two disks are orientated with their (101) and (001) surfaces facing each other after being translated by s. (c) Rotation of the (001) disk relative to the (101) disk at angle α. (d) An illustration of a typical anatase disk. Reproduced with permission.[298] Copyright 2022.
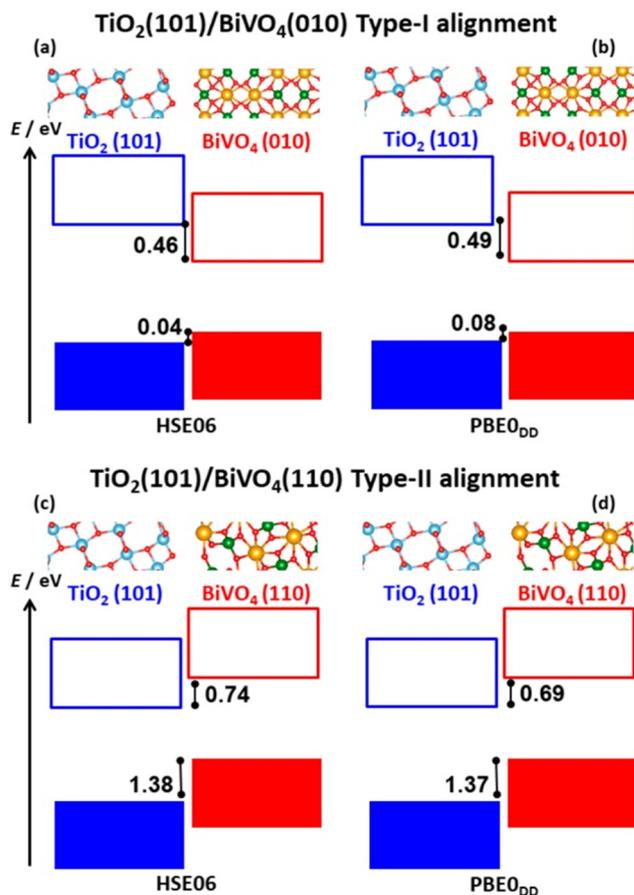

Fig. 7 (a) and (b) Schematic representation for the band alignment of TiO$_2$ (101) and BiVO$_4$ (010) with two different hybrid functionals. (c) and (d) Schematic representation for the band alignment of TiO$_2$ (101) and BiVO$_4$ (110). Reproduced with permission.[299] Copyright 2020, IOP Publishing Ltd.

points for more elaborated geometry optimizations with quantum chemical approaches.[298]

Another important and more subtle aspect in the modeling of interfaces is the surface termination. When combining two materials and creating an interface, the nature of the interaction strongly depends on the surfaces considered. In some cases, the effect determines the type of alignment of the band edges. The key example is the BiVO$_4$/TiO$_2$ heterojunction. Compelling experimental evidence was reported suggesting that the photocatalytic performances of TiO$_2$/BiVO$_4$ heterojunctions vary upon the exposure of the facet, Fig. 7. More specifically, the TiO$_2$(101)/BiVO$_4$(110) interface outperforms the TiO$_2$(101)/BiVO$_4$(010) one.[299] Quantum chemical calculations showed that the BiVO$_4$ band edges are higher than those of TiO$_2$ in the TiO$_2$(101)/BiVO$_4$(110) interface leading to a type II alignment. If

BiVO$_4$(010) is considered, then the system is predicted to have a type-I alignment.

Similar theoretical studies have been reported for Si/anatase TiO$_2$,[300] GaN/black phosphorus,[301] and ZnO/BeCdO heterojunctions.[302] The matching of the interface is so important, such that in some cases, the way the two units are terminated determines the properties of the interface. For instance, quantum chemical calculations showed that the BiOIO$_3$(010)/(100) surface junction cannot be made by the direct interaction of the two most stable terminations of the two surfaces.[296] This would lead to a band alignment not compatible with experimental evidence, Fig. 8. In this case, the formation of the interface leads to the formation of new chemical bonds, promoting a metastable termination of one surface. This allows reconciling the electronic structure of the material with its photoactivity.

Crucially, strain engineering is also employed to adjust and enhance a range of material characteristics in order to control the electrical characteristics and promote charge separation across the heterojunction.[303–305] For instance, the calculations of Yang et al. showed a negligible effect (less than 0.1 eV in total energy) of a 5% compressive strain of
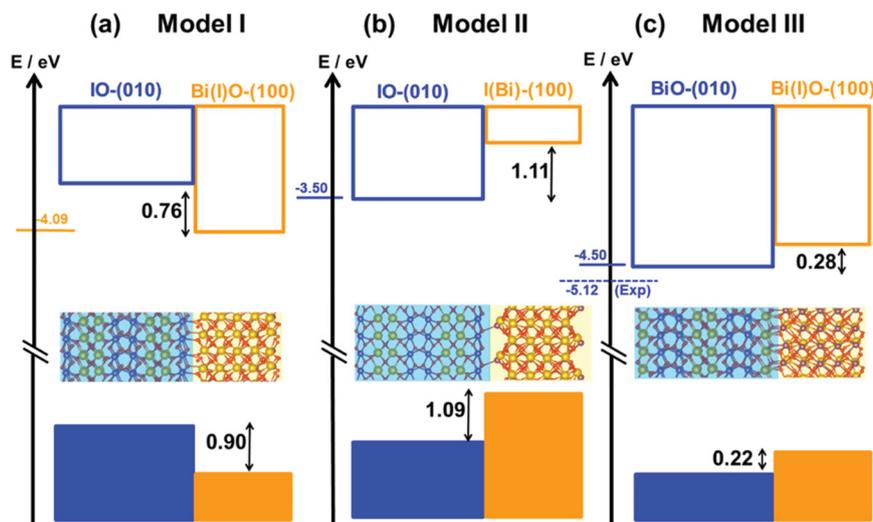
© 2025 The Author(s). Published by the Royal Society of Chemistry

RSC Appl. Interfaces, 2025, **2**, 897–916 | **905**

Fig. 8 Systematic representation of band alignment for BiOIO$_3$ interfaces with different surface terminations: (a–c) model I, model II and model III interfaces. Labeling of atoms: orange: Bi; red: O; purple: I. The two nanostructures that make up the mixed systems are distinguished by their light blue and orange areas. The experimental CBM is indicated by the horizontal dashed line. Reproduced with permission.[296] Copyright 1999–2025 John Wiley & Sons.

the MoS$_2$/ZnO heterojunction. The finding also shows that with increasing tensile biaxial strain, the spectrum's absorption edge gradually moves to the infrared region, while compressive biaxial strain causes the spectrum to blue-shift.[306] In another study, Quan Li *et al.* constructed bilayer and trilayer heterojunctions of WS$_2$/C$_2$N, WS$_2$/C$_2$N/WS$_2$, and C$_2$N/WS$_2$/C$_2$N in which biaxial strain can affect the band gap.[307]

On the other hand, the buffer layer mechanism is also an important strategy to improve photocatalytic activity in heterojunctions.[308,309] Recently, Nguyen Dinh Lam *et al.* proposed a p-Si/p-CuO buffer layer/n-ZnO heterojunction, where the addition of a 250 nm thick CuO buffer layer is beneficial for the activity. In addition, the pseudo-order rate constant (*k*) was improved by up to 12% in comparison with the p-Si/n-ZnO composite film.[310] Similar studies focused on CZTSSe/Zn(O,S),[311] ZnO/ZnS/g-C$_3$N$_4$,[190] and ZnO/CuO/g-C$_3$N$_4$.[312]

4. Electronic properties

In the construction of an interface, first-principles investigation plays an important role in determining electronic properties such as charge separation, band offsets and interface polarization.

4.1. Band edges and band offsets

In the modeling of an interface, the evaluation of the band offsets is essential. This allows determining the nature of the band edge alignment. The most popular method relies on the electrostatic potential line-up approach, which calculates the plane-averaged electrostatic potential (*V*) of the heterostructure and separated components. The conduction band minimum (CBM) and valence band maximum (VBM) of

the composing units are then aligned using the macroscopic average or stationary points of *V* as a common reference.[308,313,314] An alternative approach uses as a reference core energy levels of specific atoms.[315,316]

More specifically, the VBM and CBM of the bulk composing units (VBM$_1$, CBM$_1$) and (VBM$_2$, CBM$_2$), are aligned using a common reference, which can be taken as the macroscopic average of *V*, the band offsets are defined as:

$$VBO = (VBM_1 - \bar{V}_1) - (VBM_2 - \bar{V}_2) - (\bar{V}_1^{Het} - \bar{V}_2^{Het}) \quad (1)$$

$$CBO = (CBM_1 - \bar{V}_1) - (CBM_2 - \bar{V}_2) - (\bar{V}_1^{Het} - \bar{V}_2^{Het}) \quad (2)$$

where $\bar{V}_1$ and $\bar{V}_2$ are the macroscopic averages of the separated components, and $\bar{V}_1^{Het}$ and $\bar{V}_2^{Het}$ are the same for the composite model. Importantly, the electrostatic potential may display oscillations introducing some uncertainty, and its convergence should be checked, especially in the case of insufficiently thick models.

A very similar approach has been proposed by Conesa, and is based on the use of the stationary points of the electrostatic potential.[317] This method allows also overcoming the problem of the potential convergence. In this case, one does not need to evaluate the macroscopic average of the electrostatic potential since the stationary points, as the maxima, are directly taken as a reference.[317]

The band offsets can be calculated also by defining other common references, such as the energy of the core levels, *e.g.* the 1s orbitals, E_{1s}.[315,318] Core level energies are usually adopted as a reference in XPS measurements.[315,318–324] In this case, $\bar{V}_1$ and $\bar{V}_2$ are replaced with $E_{1,1s}$ and $E_{2,1s}$, and $\bar{V}_1^{Het}$ and $\bar{V}_2^{Het}$ with $E_{1,1s}^{Het}$ and $E_{2,1s}^{Het}$. The band offsets become:

$$VBO = (VBM_1 - E_{1,1s}) - (VBM_2 - E_{2,1s}) - (E_{1,1s}^{Het} - E_{2,1s}^{Het}) \quad (3)$$

$$CBO = (CBM_1 - E_{1,1S}) - (CBM_2 - E_{2,1S}) - (E_{1,1S}^{Het} - E_{2,1S}^{Het}) \quad (4)$$

By using core levels, it is possible to avoid the calculations of a plane-average electrostatic potential. This allows the methodology to be applied to both thick surfaces and ultrathin films. The energy of the core levels must be carefully considered because it is dependent on the chemical environment, and it may be necessary to properly compute the shifts in order to account for the relaxation of charged cells.[325–327] This contribution, which introduces an inevitable uncertainty, is typically overlooked. Illas and co-workers have thoroughly examined the precision of core level binding energies using PAW-based computations, in which the atomic cores are maintained frozen.[325]

Fig. 9 reports the case of the $SrTiO_3(001)/TiO_2(001)$ interface, where the calculated valence band offset (VBO) changes from 0.28 to 0.37 eV and the conduction band offset (CBO) from 0.03 to 0.14 eV compared to the isolated slab (depicted in Fig. 9a and b).

In another combined experimental and theoretical heterojunction investigation on $WO_3(001)/BiVO_4(010)$, the heterojunction forms a stable interface with favorable band alignment and smooth charge transfer due to small lattice mismatch at the interface, which allows us to attain high efficiency. Similar work has been applied to ZnCoMOF/g-C_3N_4,[328] N-ZnO-g-C_3N_4,[329] and g-C_3N_4/$ZnIn_2S_4$.[330]

4.2. Interface polarization

In the construction of S-scheme heterojunctions, interface polarization at the junction plays an important role in efficient charge separation. Engineering a semiconductor heterojunction in consideration of an internal electric field allows clearly identifying the route for charge transfer for efficient charge separation to minimize the recombination.[331–335]

The fundamental principle of heterojunction modeling between semiconductors is based on two different semiconductors which are directly in contact. As an example, shown in Fig. 10a, a positive charge is left behind by each electron from the n-type semiconductor that diffuses into the p-type semiconductor; a negative charge is left behind by a hole that migrates from the p-type semiconductor to the n-type semiconductor. Diffusion of electrons and holes persists until the system reaches equilibrium. Consequently, a charged area known as the "internal electric field" develops near the p–n contact. As depicted in Fig. 10b, upon sunlight illumination, the photoinduced electrons migrate from a higher CB to a lower CB and holes transfer from a low VB to a high VB which is facilitated by formation of an internal electric field (IEF) which further keeps the e–h pairs well separated.[23,25]

To make an example, Wang et al. reported a study on an S-scheme $BiOBr(002)/NiO(200)$ heterojunction for CO_2 photoreduction. NiO nanosheets with hierarchical porous structures result in enhanced light absorption due to their surface area increment. In addition, efficient charge separation is expected with the effect of electric field creation at the interface.

From the first-principles optimization, NiO possesses a band edge higher in energy and can be conceived as a reductive photocatalyst, while BiOBr with a lower band edge can be conceived as an oxidative photocatalyst. Workfunction computation and in situ irradiation X-ray photoelectron spectroscopy results show that the photoexcited electrons migrated from BiOBr to NiO through the S-scheme system, which results in strong redox ability and charge separation. When NiO and BiOBr come into contact, their electrons will move to BiOBr, Fig. 11a and b. At the interface, depletion thus leaves the interface polarized. As a result, a strong IEF that points from NiO to BiOBr is created.

Upon illumination of light, low energy photoexcited electrons in the CB of BiOBr will combine with low energy
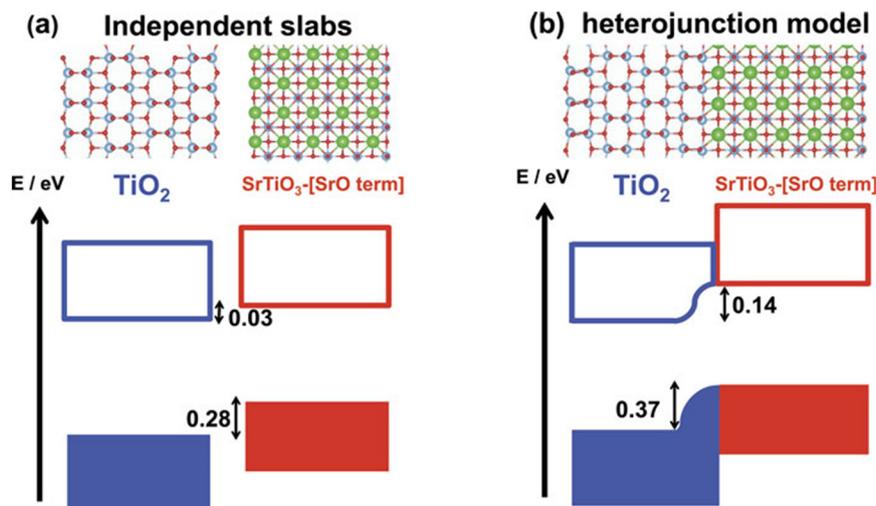

Fig. 9 Band offsets for the $SrTiO_3/TiO_2$ scheme where $TiO_2(001)$ is in contact with a SrO layer of $SrTiO_3(001)$. (a) Individual slabs. (b) The result obtained from the heterojunction model. Reproduced with permission.[319] Copyright 2020 AIP Publishing LLC.

© 2025 The Author(s). Published by the Royal Society of Chemistry

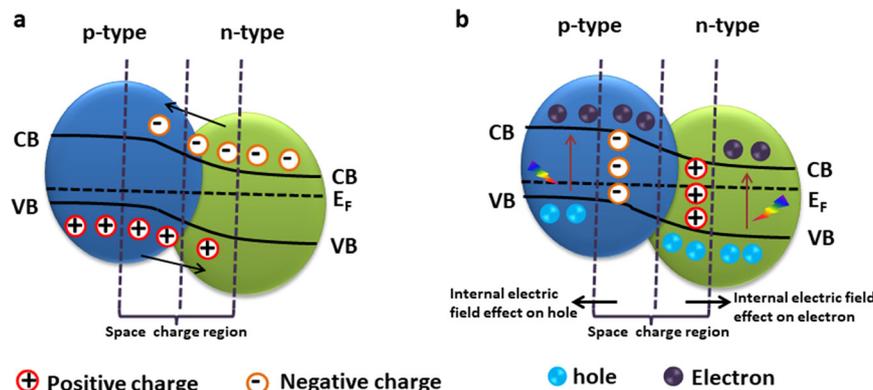RSC Appl. Interfaces, 2025, **2**, 897–916 | **907**

Fig. 10 (a) Diagram showing a p–n junction between two semiconductors. (b) Electron–hole separation with an effect of the IEF in a type II p–n junction photocatalyst upon light illumination.
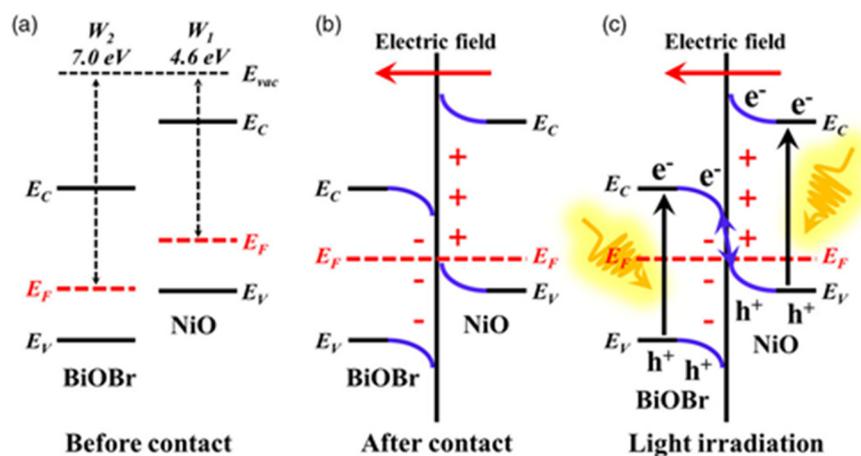

Fig. 11 a) The band structure of BiOBr and NiO. b) Formation of an IEF between BiOBr and NiO. c) Electron transfer system of the BiOBr/NiO junction under visible light illumination. Reproduced with permission.[336] Copyright 1999–2025 John Wiley & Sons.

holes in the VB of NiO while preserving high energy holes and electrons of BiOBr and NiO, respectively, Fig. 11c. On the other hand, the CO_2 photoreduction process takes place on the surface of NiO.[336] Similar work can be found in GeC/SGaSnP[335,337] and others.[338] Additional studies on the effects of the IEF and interface polarization can be referenced from BiOCl/TiO$_2$,[339] C$_2$N/α-In$_2$Se$_3$,[340] CH$_3$NH$_3$PbI$_3$/TiO$_2$,[341,342] CdS/WS$_2$,[343] BP/Bi$_2$WO$_6$,[344] HCa$_2$Nb$_3$O$_{10}$/g-C$_3$N$_4$,[345] and MoO$_3$–Bi$_4$TaO$_8$Cl.[346]

5. Conclusion and outlook

In this perspective, we presented a tutorial summary on the modeling of heterojunction materials with quantum chemical approaches. We first recalled the main archetypes of heterojunction-based materials by reporting a series of experimental studies. Then, we revised a series of fundamental ingredients to model heterojunctions. First, we discussed the crucial role of the interface model, focusing on the minimization of the lattice mismatch, the role of the surfaces in contact and their termination to the nature of the system including strain engineering and buffer layer creation.

Once the importance of the structural model was analysed, we discussed how to determine the band offsets, which in turn determine the type of band edge alignment, the primary actors for improving the separation of charge carriers upon photoexcitation. Finally, we discussed the interface polarization, as the formation (and its direction) of an interface dipole can determine the nature of the heterojunction system.

Importantly, hybrid functionals are important to accurately determine the band gap and band edge positions for the individual semiconductors and also the heterojunction. Moreover, the lattice mismatch at the interface, which causes strain in the system, should be carefully taken into account while modeling a heterojunction. Electronic properties, such as band edges and offsets, and charge migration are all directly impacted by the lattice mismatch at the interface. In principle, one should work with the lowest possible lattice mismatch, ideally close to zero. If not possible, it is important to check for the spurious effects induced by the working strain.

Once the heterojunction model is obtained, other aspects like the direction of charge polarization must be considered. It

908 | *RSC Appl. Interfaces*, 2025, **2**, 897–916

© 2025 The Author(s). Published by the Royal Society of Chemistry

is worth mentioning that the presence of buffer layers in certain systems can be utilized to change the band alignment's nature and charge polarization. In addition, considering strain engineering is important to manage the electrical characteristics and encourage charge space separation across the heterojunction. We finally highlight that the information extracted from heterojunction models is obtained from "nearly" ideal systems. A possible strategy to scale-up the computational models is to invoke multi-scale approaches to reduce the gap between the complexity of experiments and the theoretical models. We hope that this review could help in modeling novel heterojunction materials and existing ones for which atomistic explanation is still missing.

Data availability

The data reported in this manuscript can be found in the mentioned references. No new data were produced in this work.

Conflicts of interest

The authors declare no conflicts of interest.

Acknowledgements

References

1 P. A. Owusu and S. Asumadu-Sarkodie, *Cogent Eng.*, 2016, **3**(1), 1167990.

2 S. J. A. Moniz, S. A. Shevlin, D. J. Martin, Z.-X. Guo and J. Tang, *Energy Environ. Sci.*, 2015, **8**(3), 731–759.

3 S. Li, W. Xu, L. Meng, W. Tian and L. Li, *Small Sci.*, 2022, **2**(5), 2100112.

4 A. Fujishima and K. Honda, *Nature*, 1972, **238**(5358), 37–38.

5 D. J. Martin, P. J. Reardon, S. J. Moniz and J. Tang, *J. Am. Chem. Soc.*, 2014, **136**(36), 12568–12571.

6 X. Yang and D. Wang, *ACS Appl. Energy Mater.*, 2018, **1**(12), 6657–6693.

7 E. Dupont, R. Koppelaar and H. Jeanmart, *Appl. Energy*, 2020, **257**, 113968.

8 M. Melchionna and P. Fornasiero, *ACS Catal.*, 2020, **10**(10), 5493–5501.

9 X. Zhang, S. Xiong, A. Sathiyaseelan, L. Zhang, Y. Lu, Y. Chen, T. Jin and M. H. Wang, *Chemosphere*, 2024, **364**, 143142.

10 L. Chen, Z. Liu, Z. Guo and X.-J. Huang, *J. Mater. Chem. A*, 2020, **8**(34), 17326–17359.

11 A. Balapure, J. Ray Dutta and R. Ganesan, *RSC Appl. Interfaces*, 2024, **1**(1), 43–69.

12 M. Humayun, C. Wang and W. Luo, *Small Methods*, 2022, **6**(2), e2101395.

13 F. Liu, C. Shi, X. Guo, Z. He, L. Pan, Z. F. Huang, X. Zhang and J. J. Zou, *Adv. Sci.*, 2022, **9**(18), e2200307.

14 Y. Wang, H. Suzuki, J. Xie, O. Tomita, D. J. Martin, M. Higashi, D. Kong, R. Abe and J. Tang, *Chem. Rev.*, 2018, **118**(10), 5201–5241.

15 N. Goodarzi, Z. Ashrafi-Peyman, E. Khani and A. Z. Moshfegh, *Catalysts*, 2023, **13**(7), 1102.

16 H. Mai, D. Chen, Y. Tachibana, H. Suzuki, R. Abe and R. A. Caruso, *Chem. Soc. Rev.*, 2021, **50**(24), 13692–13729.

17 A. Rahman and M. M. Khan, *New J. Chem.*, 2021, **45**(42), 19622–19635.

18 Q. Guo, C. Zhou, Z. Ma and X. Yang, *Adv. Mater.*, 2019, **31**(50), e1901997.

19 R. Saffari, Z. Shariatinia and M. Jourshabani, *Environ. Pollut.*, 2020, **259**, 113902.

20 P. Singh, R. Kumar and R. K. Singh, *Ind. Eng. Chem. Res.*, 2019, **58**(37), 17130–17163.

21 S. Rej, M. Bisetto, A. Naldoni and P. Fornasiero, *J. Mater. Chem. A*, 2021, **9**(10), 5915–5951.

22 B. A. Koiki and O. A. Arotiba, *RSC Adv.*, 2020, **10**(60), 36514–36525.

23 S. Bai, J. Jiang, Q. Zhang and Y. Xiong, *Chem. Soc. Rev.*, 2015, **44**(10), 2893–2939.

24 X. Shi, L. Mao, P. Yang, H. Zheng, M. Fujitsuka, J. Zhang and T. Majima, *Appl. Catal., B*, 2020, **265**, 118616.

25 M. Eshete, X. Li, L. Yang, X. Wang, J. Zhang, L. Xie, L. Deng, G. Zhang and J. Jiang, *Small Sci.*, 2023, **3**(3), 2200041.

26 J. Ma, J. Low, J. Zhang and J. Yu, *Semicon. Sol. Photocatal.*, 2021, pp. 71–100.

27 P. Kumari, N. Bahadur, L. Kong, L. A. O'Dell, A. Merenda and L. F. Dumée, *Mater. Adv.*, 2022, **3**(5), 2309–2323.

28 A. Wang, S. Wu, J. Dong, R. Wang, J. Wang, J. Zhang, S. Zhong and S. Bai, *Chem. Eng. J.*, 2021, **404**, 127145.

29 Z. Wang, C. Li and K. Domen, *Chem. Soc. Rev.*, 2019, **48**(7), 2109–2125.

30 Q. Xu, S. Wageh, A. A. Al-Ghamdi and X. Li, *J. Mater. Sci. Technol.*, 2022, **124**, 171–173.

31 Z. Xiong, Q. Liu, Z. Gao, J. Yang, X. Zhang, Q. Yang and C. Hao, *Inorg. Chem.*, 2021, **60**(7), 5063–5070.

32 H. Li, H. Yu, X. Quan, S. Chen and H. Zhao, *Adv. Funct. Mater.*, 2015, **25**(20), 3074–3080.

33 L. Wei, C. Yu, Q. Zhang, H. Liu and Y. Wang, *J. Mater. Chem. A*, 2018, **6**(45), 22411–22436.

34 F. Chen, Y. Wei, M. Ren, S. Sun, S. Ghosh and R. V. Kumar, *ChemCatChem*, 2024, **16**(10), e202301492.

35 X. Li, C. Garlisi, Q. Guan, S. Anwer, K. Al-Ali, G. Palmisano and L. Zheng, *Mater. Today*, 2021, **47**, 75–107.

36 X. Li, H. Jiang, C. Ma, Z. Zhu, X. Song, H. Wang, P. Huo and X. Li, *Appl. Catal., B*, 2021, **283**, 119638.

37 X. Wan, Y. Gao, M. Eshete, M. Hu, R. Pan, H. Wang, L. Liu, J. Liu, J. Jiang, S. Brovelli and J. Zhang, *Nano Energy*, 2022, **98**, 107217.

38 L. Schumacher and R. Marschall, *Top. Curr. Chem.*, 2022, **380**(6), 53.

39 L. Wang, B. Zhu, J. Zhang, J. B. Ghasemi, M. Mousavi and J. Yu, *Matter*, 2022, **5**(12), 4187–4211.

40 M. J. Molaei, *J. Am. Ceram. Soc.*, 2024, **107**(9), 5695–5719.

© 2025 The Author(s). Published by the Royal Society of Chemistry

RSC Appl. Interfaces, 2025, **2**, 897–916 | **909**

41 A. B. Trench, R. Alvarez, V. Teodoro, L. G. da Trindade, T. R. Machado, M. M. Teixeira, D. de Souza, I. M. Pinatti, A. Z. Simões, Y. G. Gobato, J. Andrés and E. Longo, *Mater. Chem. Phys.*, 2022, **280**, 125710.

42 L. Che, J. Pan, K. Cai, Y. Cong and S.-W. Lv, *Sep. Purif. Technol.*, 2023, **315**, 123708.

43 H. Lüth, *Sol. Surf. Interfaces and Thin Films*, 2015, pp. 393–448.

44 J. Tyczkowski and H. Kierzkowska-Pawlak, *ACS Appl. Mater. Interfaces*, 2024, **16**(29), 37339–37345.

45 L. Wang, W. Wang, Y. Chen, L. Yao, X. Zhao, H. Shi, M. Cao and Y. Liang, *ACS Appl. Mater. Interfaces*, 2018, **10**(14), 11652–11662.

46 L. Liccardo, E. Lushaj, L. Dal Compare, E. Moretti and A. Vomiero, *Small Sci.*, 2022, **2**(3), 2270006.

47 K. Wang, Y. Zhang, L. Liu, N. Lu and Z. Zhang, *J. Mater. Sci.*, 2019, **54**(11), 8426–8435.

48 S. Joshi, R. K. Canjeevaram Balasubramanyam, S. J. Ippolito, Y. M. Sabri, A. E. Kandjani, S. K. Bhargava and M. V. Sunkara, *ACS Appl. Nano Mater.*, 2018, **1**(7), 3375–3388.

49 U. Saeed, A. Jilani, J. Iqbal and H. Al-Turaif, *Inorg. Chem. Commun.*, 2022, **142**, 109623.

50 M. Ding, H. Yang, T. Yan, C. Wang, X. Deng, S. Zhang, J. Huang, M. Shao and X. Xu, *Nanoscale Res. Lett.*, 2018, **13**(1), 260.

51 B. Babu, V. V. N. Harish, J. Shim and C. V. Reddy, *J. Mater. Sci.: Mater. Electron.*, 2018, **29**(19), 16988–16996.

52 C. Xu, C. Jin, W. Chang, X. Hu, H. Deng, E. Liu and J. Fan, *Catal. Sci. Technol.*, 2019, **9**(18), 4990–5000.

53 S. Seo, S. Kim, H. Choi, J. Lee, H. Yoon, G. Piao, J.-C. Park, Y. Jung, J. Song, S. Y. Jeong, H. Park and S. Lee, *Adv. Sci.*, 2019, **6**(13), 1900301.

54 K. Hernandez Ruiz, Z. Wang, M. Ciprian, M. Zhu, R. Tu, L. Zhang, W. Luo, Y. Fan and W. Jiang, *Small Sci.*, 2022, **2**(1), 2100047.

55 P. A. Bharad, A. V. Nikam, F. Thomas and C. S. Gopinath, *ChemistrySelect*, 2018, **3**(43), 12022–12030.

56 G. Li, J. Huang, J. Chen, Z. Deng, Q. Huang, Z. Liu, W. Guo and R. Cao, *ACS Omega*, 2019, **4**(2), 3392–3397.

57 V. V. Pham, D. P. Bui, H. H. Tran, M. T. Cao, T. K. Nguyen, Y. S. Kim and V. H. Le, *RSC Adv.*, 2018, **8**(22), 12420–12427.

58 L. Xinkun, P. Guo, R. Li, J. Liu and M. Huang, *Russ. J. Phys. Chem. A*, 2019, **93**(3), 515–521.

59 F. Liu, C. Chen, Q. Zhang, Z. Zhang and X. Fang, *Nanoscale*, 2022, **14**(32), 11664–11675.

60 Y. Dong, S.-Y. Chen, Y. Lu, Y.-X. Xiao, J. Hu, S.-M. Wu, Z. Deng, G. Tian, G.-G. Chang, J. Li, S. Lenaerts, C. Janiak, X.-Y. Yang and B.-L. Su, *Chem. – Asian J.*, 2018, **13**(12), 1609–1615.

61 X. Yang, G. Lu, B. Wang, T. Wang and Y. Wang, *RSC Adv.*, 2019, **9**(43), 25142–25150.

62 M. Humayun, Z. Zheng, Q. Fu and W. Luo, *Environ. Sci. Pollut. Res.*, 2019, **26**(17), 17696–17706.

63 K. Zhou, P. Li, Y. Zhu, X. Ye, H. Chen, Y. Yang, Y. Dan, Y. Yuan and H. Hou, *Catal. Lett.*, 2021, **151**(1), 78–85.

64 S. Liu, J. Chen, D. Liu, L. Shan and X. Zhang, *J. Nanopart. Res.*, 2019, **21**(8), 191.

65 Z. Mu, S. Chen, Y. Wang, Z. Zhang, Z. Li, B. Xin and L. Jing, *Small Sci.*, 2021, **1**(10), 2100050.

66 T. Qiu, S. Liu, H. Cai, Y. Zhou, K. Chen, Y. Huang and Q. Feng, *J. Mater. Sci.: Mater. Electron.*, 2018, **29**(20), 17463–17472.

67 J. Zhuang, J. Liu, Z. Wu, Z. Li, K. Zhu, K. Yan, Y. Xu, Y. Huang and Z. Lin, *J. Mater. Sci.: Mater. Electron.*, 2019, **30**(12), 11368–11377.

68 A.-A. Hoseini, S. Farhadi, A. Zabardasti and F. Siadatnasab, *RSC Adv.*, 2019, **9**(42), 24489–24504.

69 L. Zhang, L. Zhuang, H. Liu, L. Zhang, R. Cai, N. Chen, X. Yang, Z. Zhu, D. Yang and X. Yao, *Small Sci.*, 2021, **1**(4), 2000027.

70 L. Zhu, H. Li, Z. Liu, P. Xia, Y. Xie and D. Xiong, *J. Phys. Chem. C*, 2018, **122**(17), 9531–9539.

71 Y. T. Prabhu, V. Navakoteswara Rao, M. V. Shankar, B. Sreedhar and U. Pal, *New J. Chem.*, 2019, **43**(17), 6794–6805.

72 X. Y. Sun, X. Zhang, X. Sun, C. Liu, N. X. Qian, R. Rao, M. Wang and Y. Q. Ma, *Appl. Organomet. Chem.*, 2019, **33**(11), e5173.

73 M. Zahoor, A. Arshad, Y. Khan, M. Iqbal, S. Z. Bajwa, R. A. Soomro, I. Ahmad, F. K. Butt, M. Z. Iqbal, A. Wu and W. S. Khan, *Appl. Nanosci.*, 2018, **8**(5), 1091–1099.

74 M. Chandra, K. Bhunia and D. Pradhan, *Inorg. Chem.*, 2018, **57**(8), 4524–4533.

75 S.-S. Yi, B.-R. Wulan, J.-M. Yan and Q. Jiang, *Adv. Funct. Mater.*, 2019, **29**(11), 1801902.

76 Y. Zeng, N. Guo, H. Li, Q. Wang, X. Xu, Y. Yu, X. Han and H. Yu, *Chem. Commun.*, 2019, **55**(5), 683–686.

77 M. Rajesh Kumar, G. Murugadoss, A. N. Pirogov and R. Thangamuthu, *J. Mater. Sci.: Mater. Electron.*, 2018, **29**(16), 13508–13515.

78 S. Jayswal and R. S. Moirangthem, *New J. Chem.*, 2018, **42**(16), 13689–13701.

79 K. Maeda, *ACS Catal.*, 2013, **3**(7), 1486–1503.

80 H. Yang, *Mater. Res. Bull.*, 2021, **142**, 111406.

81 J. Wang, B. Wang, W. Zhang, Y. Xiao, H. Xu, Y. Liu, Z. Liu, J. Zhang and Y. Jiang, *Appl. Surf. Sci.*, 2022, **587**, 152867.

82 Q. Dong, Z. Chen, B. Zhao, Y. Zhang, Z. Lu, X. Wang, J. Li and W. Chen, *J. Colloid Interface Sci.*, 2022, **608**(Pt 2), 1951–1959.

83 Z. Xing, S. Shen, M. Wang, F. Ren, Y. Liu, X. Zheng, Y. Liu, X. Xiao, W. Wu and C. Jiang, *Appl. Phys. Lett.*, 2014, **105**(14), 143902.

84 H. Li, W. Tu, Y. Zhou and Z. Zou, *Adv. Sci.*, 2016, **3**(11), 1500389.

85 A. Nakada, R. Kuriki, K. Sekizawa, S. Nishioka, J. J. M. Vequizo, T. Uchiyama, N. Kawakami, D. Lu, A. Yamakata, Y. Uchimoto, O. Ishitani and K. Maeda, *ACS Catal.*, 2018, **8**(10), 9744–9754.

86 J. Bao, Y. Chen, W. Li, J. Zhang, F. Zeng, L. Liu and G. Tian, *J. Mater. Chem. A*, 2025, **13**, 5365–5373.

87 E. Aguilera-Ruiz, M. de la Garza-Galván, P. Zambrano-Robledo, J. C. Ballesteros-Pacheco, J. Vazquez-Arenas, J.

910 | *RSC Appl. Interfaces*, 2025, **2**, 897–916

© 2025 The Author(s). Published by the Royal Society of Chemistry

Peral and U. M. García-Pérez, *RSC Adv.*, 2017, **7**(73), 45885–45895.

88 N. Khan, F. Stelo, G. H. C. Santos, L. M. Rossi, R. V. Gonçalves and H. Wender, *Appl. Surf. Sci. Adv.*, 2022, **11**, 100289.

89 S. Zheng, P. Lu, A. M. Idris, B. Chen, X. Jiang, G. Jiang, J. Wang, S. Li and Z. Li, *J. Mater. Chem. A*, 2025, **13**, 5346–5356.

90 X. Li, D. Chen, N. Li, Q. Xu, H. Li, J. He and J. Lu, *J. Alloys Compd.*, 2020, **843**, 155772.

91 C. Lu, F. Guo, Q. Yan, Z. Zhang, D. Li, L. Wang and Y. Zhou, *J. Alloys Compd.*, 2019, **811**, 151976.

92 G. Zuo, Y. Wang, W. L. Teo, Q. Xian and Y. Zhao, *Appl. Catal., B*, 2021, **291**, 120126.

93 Z. Liang, B. Ouyang, T. Wang, X. Liu, H. Huo, D. Liu, H. Feng, J. Ma, K. Deng, A. Li and E. Kan, *Int. J. Hydrogen Energy*, 2022, **47**(20), 10868–10876.

94 N. R. Khalid, M. K. Hussain, G. Murtaza, M. Ikram, M. Ahmad and A. Hammad, *J. Inorg. Organomet. Polym. Mater.*, 2019, **29**(4), 1288–1296.

95 S. Du, C. Li, X. Lin, W. Xu, X. Huang, H. Xu and P. Fang, *ChemPlusChem*, 2019, **84**(7), 999–1010.

96 R. E. Adam, M. Pirhashemi, S. Elhag, X. Liu, A. Habibi-Yangjeh, M. Willander and O. Nur, *RSC Adv.*, 2019, **9**(15), 8271–8279.

97 M. Wang, Q. Han, L. Li, L. Tang, H. Li, Y. Zhou and Z. Zou, *Nanotechnology*, 2017, **28**(27), 274002.

98 C. Wang, Y. Zhao, H. Xu, Y. Li, Y. Wei, J. Liu and Z. Zhao, *Appl. Catal., B*, 2020, 263.

99 M. Liang, T. Borjigin, Y. Zhang, H. Liu, B. Liu and H. Guo, *ACS Appl. Mater. Interfaces*, 2018, **10**(40), 34123–34131.

100 J. Li, X. Yang, C. Ma, Y. Lei, Z. Cheng and Z. Rui, *Appl. Catal., B*, 2021, **291**, 120053.

101 C. Zhou, S. Wang, Z. Zhao, Z. Shi, S. Yan and Z. Zou, *Adv. Funct. Mater.*, 2018, **28**(31), 1801214.

102 J. Li, J. Chen, H. Fang, X. Guo and Z. Rui, *Ind. Eng. Chem. Res.*, 2021, **60**(23), 8420–8429.

103 J. Yang, C. Shi, Y. Dong, H. Su, H. Sun, Y. Guo and S. Yin, *J. Colloid Interface Sci.*, 2022, **605**, 373–384.

104 K. Ouyang, B. Xu, C. Yang, H. Wang, P. Zhan and S. Xie, *Mater. Sci. Semicond. Process.*, 2022, **137**, 106168.

105 B. Ju, F. Yang, K. Huang and Y. Wang, *J. Alloys Compd.*, 2020, **815**, 151886.

106 N. Lu, X. Jing, J. Zhang, P. Zhang, Q. Qiao and Z. Zhang, *Chem. Eng. J.*, 2022, **431**, 134001.

107 S. Yao, R. Zheng, R. Li, Y. Chen, X. Zhou and J. Luo, *J. Taiwan Inst. Chem. Eng.*, 2019, **100**, 186–193.

108 Q. Xu, L. Zhang, B. Cheng, J. Fan and J. Yu, *Chem*, 2020, **6**(7), 1543–1559.

109 F. Li, G. Zhu, J. Jiang, L. Yang, F. Deng and X. Li, *J. Mater. Sci. Technol.*, 2024, **177**, 142–180.

110 X. Hao, D. Xiang and Z. Jin, *ChemCatChem*, 2021, **13**(22), 4738–4750.

111 R. Shen, X. Lu, Q. Zheng, Q. Chen, Y. H. Ng, P. Zhang and X. Li, *Sol. RRL*, 2021, **5**(7), 2100177.

112 K. A. Alzahrani and A. A. Ismail, *Surf. Interfaces*, 2023, **39**, 102935.

113 W. Bootluck, T. Chittrakarn, K. Techato, P. Jutaporn and W. Khongnakorn, *Catal. Lett.*, 2022, **152**(9), 2590–2606.

114 J. Zhu, Q. Bi, Y. Tao, W. Guo, J. Fan, Y. Min and G. Li, *Adv. Funct. Mater.*, 2023, **33**(15), 2213131.

115 Y. Song, J. Zhang, X. Dong and H. Li, *Energy Technol.*, 2021, **9**(5), 2100033.

116 J. Li, C. Wu, J. Li, B. Dong, L. Zhao and S. Wang, *Chin. J. Catal.*, 2022, **43**(2), 339–349.

117 X. Wu, G. Chen, L. Li, J. Wang and G. Wang, *J. Mater. Sci. Technol.*, 2023, **167**, 184–204.

118 G. Zhang, H. Wu, D. Chen, N. Li, Q. Xu, H. Li, J. He and J. Lu, *Green Energy Environ.*, 2022, **7**(2), 176–204.

119 M. Dai, Z. He, P. Zhang, X. Li and S. Wang, *J. Mater. Sci. Technol.*, 2022, **122**, 231–242.

120 C. Liu, S. Mao, H. Wang, Y. Wu, F. Wang, M. Xia and Q. Chen, *Chem. Eng. J.*, 2022, **430**, 132806.

121 Y. Chen, J. Huang, J. Zhong, M. Li, Z. Li and C. Yang, *Chem. Phys. Lett.*, 2021, **780**, 138966.

122 K. Wang, X. Shao, K. Zhang, J. Wang, X. Wu and H. Wang, *Appl. Surf. Sci.*, 2022, **596**, 153444.

123 Z. Jin, X. Jiang and X. Guo, *Int. J. Hydrogen Energy*, 2022, **47**(3), 1669–1682.

124 J. Li, M. Li and Z. Jin, *J. Colloid Interface Sci.*, 2021, **592**, 237–248.

125 D.-E. Lee, N. Mameda, K. P. Reddy, B. M. Abraham, W.-K. Jo and S. Tonda, *J. Mater. Sci. Technol.*, 2023, **161**, 74–87.

126 W. Huang, W. Xue, X. Hu, J. Fan, C. Tang and E. Liu, *Appl. Surf. Sci.*, 2022, **599**, 153900.

127 J. Geng, S. Guo, Z. Zou, Z. Yuan, D. Zhang, X. Yan, X. Ning and X. Fan, *Fuel*, 2023, **333**, 126417.

128 H. Ge, F. Xu, B. Cheng, J. Yu and W. Ho, *ChemCatChem*, 2019, **11**(24), 6301–6309.

129 S. Han, B. Li, L. Huang, H. Xi, Z. Ding and J. Long, *Chin. J. Struct. Chem.*, 2022, **41**(1), 2201007–2201013.

130 J. Wang, H. Cheng, D. Wei and Z. Li, *Chin. J. Catal.*, 2022, **43**(10), 2606–2614.

131 Z. Zhang, Z. Dong, Y. Jiang, Y. Chu and J. Xu, *Chem. Eng. J.*, 2022, **435**, 135014.

132 Z. Zhang, M. Wang, Z. Chi, W. Li, H. Yu, N. Yang and H. Yu, *Appl. Catal., B*, 2022, **313**, 121426.

133 Z. Jiang, B. Cheng, Y. Zhang, S. Wageh, A. A. Al-Ghamdi, J. Yu and L. Wang, *J. Mater. Sci. Technol.*, 2022, **124**, 193–201.

134 S. Cao, J. Yu, S. Wageh, A. A. Al-Ghamdi, M. Mousavi, J. B. Ghasemi and F. Xu, *J. Mater. Chem. A*, 2022, **10**(33), 17174–17184.

135 A. Xu, W. Tu, S. Shen, Z. Lin, N. Gao and W. Zhong, *Appl. Surf. Sci.*, 2020, **528**, 146949.

136 L. Liu, T. Hu, K. Dai, J. Zhang and C. Liang, *Chin. J. Catal.*, 2021, **42**(1), 46–55.

137 J. Huang, B. Zhu, D. Song, B. Wang, L. Chen, L. Lu, Q. Chen, L. Gai, C. Zhai, L. Chen and H. Tao, *Chem. Eng. J.*, 2023, **464**, 142784.

138 J. Yang, J. Wang, W. Zhao, G. Wang, K. Wang, X. Wu and J. Li, *Appl. Surf. Sci.*, 2023, **613**, 156083.

© 2025 The Author(s). Published by the Royal Society of Chemistry

RSC Appl. Interfaces, 2025, **2**, 897–916 | **911**

139 Y. Qin, K. Xiao, S. Sun, Y. Wang and C. Kang, *Appl. Surf. Sci.*, 2023, **616**, 156431.

140 J. Piriyanon, T. Chankhanittha, S. Youngme, K. Hemavibool, S. Nijpanich, S. Juabrum, N. Chanlek and S. Nanan, *J. Mater. Sci.: Mater. Electron.*, 2021, **32**(14), 19798–19819.

141 W. Liu, X. Li, K. Qi, Y. Wang, F. Wen and J. Wang, *Appl. Surf. Sci.*, 2023, **607**, 155085.

142 X. Yue, L. Cheng, J. Fan and Q. Xiang, *Appl. Catal., B*, 2022, **304**, 120979.

143 Y. Liu, X. Hao, H. Hu and Z. Jin, *Acta Phys.-Chim. Sin.*, 2021, **37**(6), 2008030.

144 C. Chen, J. Zhou, J. Geng, R. Bao, Z. Wang, J. Xia and H. Li, *Appl. Surf. Sci.*, 2020, **503**, 144287.

145 X. Lu, L. Quan, H. Hou, J. Qian, Z. Liu and Q. Zhang, *J. Alloys Compd.*, 2022, **925**, 166552.

146 H. Fan, H. Zhou, W. Li, S. Gu and G. Zhou, *Appl. Surf. Sci.*, 2020, **504**, 144351.

147 Z. Li, D. Lan, Z. Li, J. Sun, S. Chen, J. Yang, J. Wei, Z. Yu, S. Wang and Y. Hou, *Chemosphere*, 2022, **301**, 134684.

148 B. Xia, B. He, J. Zhang, L. Li, Y. Zhang, J. Yu, J. Ran and S. Z. Qiao, *Adv. Energy Mater.*, 2022, **12**(46), 2201449.

149 J. Wu, K. Li, S. Yang, C. Song and X. Guo, *Chem. Eng. J.*, 2023, **452**, 139493.

150 M. Zhao, S. Liu, D. Chen, S. Zhang, S. A. C. Carabineiro and K. Lv, *Chin. J. Catal.*, 2022, **43**(10), 2615–2624.

151 K. Chen, Y. Shi, P. Shu, Z. Luo, W. Shi and F. Guo, *Chem. Eng. J.*, 2023, **454**, 140053.

152 Z. Miao, Q. Wang, Y. Zhang, L. Meng and X. Wang, *Appl. Catal., B*, 2022, **301**, 120802.

153 S. Zhou, C. Yang, L. Guo, R. Ali Soomro, M. Niu, Z. Yang, R. Du, D. Wang, F. Fu and B. Xu, *Appl. Surf. Sci.*, 2023, **625**, 157192.

154 S. Pang, Y. Dong, D. Xu, Q. Wang, W. Gao, L. Zhang, K. Wang, G. Zhang, L. Lv, Y. Xia, Z. Ren and P. Wang, *J. Mater. Sci. Technol.*, 2023, **158**, 145–155.

155 Z. Wang, B. Cheng, L. Zhang, J. Yu, Y. Li, S. Wageh and A. A. Al-Ghamdi, *Chin. J. Catal.*, 2022, **43**(7), 1657–1666.

156 Y. Wang, Y. Tang, J. Sun, X. Wu, H. Liang, Y. Qu and L. Jing, *Appl. Catal., B*, 2022, **319**, 121893.

157 R. Chen, J. Xia, Y. Chen and H. Shi, *Acta Phys.-Chim. Sin.*, 2022, **0**(0), 2209012.

158 J. Wang, X. Qiao, W. Shi, J. He, J. Chen and W. Zhang, *Acta Phys.-Chim. Sin.*, 2023, **39**(6), 2210003.

159 G. Han, C. Liu, Y. Pan, W. Macyk, S. Wageh, A. A. Al-Ghamdi and F. Xu, *Adv. Sustainable Syst.*, 2023, **7**(1), 2200381.

160 S. Li, M. Cai, C. Wang, Y. Liu, N. Li, P. Zhang and X. Li, *J. Mater. Sci. Technol.*, 2022, **123**, 177–190.

161 F. He, A. Meng, B. Cheng, W. Ho and J. Yu, *Chin. J. Catal.*, 2020, **41**(1), 9–20.

162 Z. Li, J. Xu, Z. Liu, X. Liu, S. Xu and Y. Ma, *Int. J. Hydrogen Energy*, 2023, **48**(9), 3466–3477.

163 M. Li, D. Zhang, H. Zhou, K. Sun, X. Ma and M. Dong, *Int. J. Hydrogen Energy*, 2023, **48**(13), 5126–5137.

164 J. Mu, F. Teng, H. Miao, Y. Wang and X. Hu, *Appl. Surf. Sci.*, 2020, **501**, 143974.

165 W. Shi, J.-C. Wang, X. Guo, X. Qiao, F. Liu, R. Li, W. Zhang, Y. Hou and H. Han, *Nano Res.*, 2022, **15**(7), 5962–5969.

166 Z. Zhao, Q. Ling, Z. Li, K. Yan, C. Ding, P. Chen, L. Yang, Z. Sun and M. Zhang, *Sep. Purif. Technol.*, 2023, **308**, 122928.

167 T. Bavani, P. Sasikala, S. Arumugam, A. Malathi, P. Praserthdam and J. Madhavan, *Environ. Sci. Pollut. Res.*, 2023, **30**(12), 34468–34480.

168 J. Chen, J. Zhong, J. Li and K. Qiu, *Appl. Surf. Sci.*, 2021, **563**, 150246.

169 M. Liu, P. Ye, M. Wang, L. Wang, C. Wu, J. Xu and Y. Chen, *J. Environ. Chem. Eng.*, 2022, **10**(5), 108436.

170 A. Shamloufard, S. Hajati, A. A. Youzbashi, K. Dashtian, M. Moradi and J. Toth, *Appl. Surf. Sci.*, 2022, **590**, 153118.

171 Z. Liu, J. Xu, C. Xiang, Y. Liu, L. Ma and L. Hu, *Appl. Surf. Sci.*, 2021, **569**, 150973.

172 K. A. Alzahrani, A. A. Ismail and N. Alahmadi, *J. Mol. Liq.*, 2023, **376**, 121509.

173 J. Wang, Q. Zhang, F. Deng, X. Luo and D. D. Dionysiou, *Chem. Eng. J.*, 2020, **379**, 122264.

174 S. Li, C. Wang, Y. Liu, M. Cai, Y. Wang, H. Zhang, Y. Guo, W. Zhao, Z. Wang and X. Chen, *Chem. Eng. J.*, 2022, **429**, 132519.

175 W. Zhao, H. Chen, J. Zhang, P. J. Low and H. Sun, *Chem. Sci.*, 2024, **15**(42), 17292–17327.

176 W. Xu, W. Tian, L. Meng, F. Cao and L. Li, *Adv. Energy Mater.*, 2021, **11**(8), 2003500.

177 V. Q. Hieu, T. C. Lam, A. Khan, T.-T. Thi Vo, T.-Q. Nguyen, V. D. Doan, D. L. Tran, V. T. Le and V. A. Tran, *Chemosphere*, 2021, **285**, 131429.

178 A. M. Taddesse, M. Alemu and T. Kebede, *J. Environ. Chem. Eng.*, 2020, **8**(5), 104356.

179 A. Bolatov, A. Manjovelo, B. Chouchene, L. Balan, T. Gries, G. Medjahdi, B. Uralbekov and R. Schneider, *Mater.*, 2024, **17**(19), 4877.

180 Q. A. Drmosh, A. Hezam, A. H. Y. Hendi, M. Qamar, Z. H. Yamani and K. Byrappa, *Appl. Surf. Sci.*, 2020, **499**, 143938.

181 K. Alkanad, A. Hezam, Q. A. Drmosh, S. S. Ganganakatte Chandrashekar, A. A. AlObaid, I. Warad, M. A. Bajiri and L. Neratur Krishnappagowda, *Sol. RRL*, 2021, **5**(11), 2100501.

182 M. Aadil, T. Kousar, M. Hussain, H. H. Somaily, A. K. Abdulla, E. R. Muhammad, E. A. Al-Abbad, M. A. Salam, S. M. Albukhari, D. F. Baamer and M. Z. Ansari, *Ceram. Int.*, 2023, **49**(3), 4846–4854.

183 S. Girma, A. M. Taddesse, Y. Bogale and Z. Bezu, *J. Photochem. Photobiol., A*, 2023, **444**, 114963.

184 A. Nawaz, S. Goudarzi, H. Zarrin and P. Saravanan, *J. Alloys Compd.*, 2022, **903**, 163951.

185 A. Hezam, K. Namratha, Q. A. Drmosh, Z. H. Yamani and K. Byrappa, *Ceram. Int.*, 2017, **43**(6), 5292–5301.

186 M. Pirhashemi and A. Habibi-Yangjeh, *Sep. Purif. Technol.*, 2018, **193**, 69–80.

187 M. Pirhashemi and A. Habibi-Yangjeh, *Mater. Chem. Phys.*, 2018, **214**, 107–119.

188 M. Shekofteh-Gohari and A. Habibi-Yangjeh, *Solid State Sci.*, 2017, **74**, 24–36.

189 M. Wang, G. Tan, H. Ren, A. Xia and Y. Liu, *Appl. Surf. Sci.*, 2019, **492**, 690–702.

190 Z. Dong, Y. Wu, N. Thirugnanam and G. Li, *Appl. Surf. Sci.*, 2018, **430**, 293–300.

191 B. Feng, Q. Wang, P. Liu, Z. Yuan, D. Pan, M. Ye, K. Shen and Z. Xin, *Nanoscale*, 2024, **16**(37), 17616–17623.

192 Y. Jiao, Y. Li, J. Wang, Z. He and Z. Li, *Appl. Surf. Sci.*, 2020, **534**, 147603.

193 Y. Cheng, P. Fu, X. Yang, Y. Zhang, S. Jin, H. Liu, Y. Shen, X. Guo and L. Chen, *J. Mater. Chem. A*, 2023, **11**(45), 24764–24776.

194 W. Xue, D. Huang, J. Li, G. Zeng, R. Deng, Y. Yang, S. Chen, Z. Li, X. Gong and B. Li, *Chem. Eng. J.*, 2019, **373**, 1144–1157.

195 A. Kumar, G. Sharma, A. Kumari, C. Guo, M. Naushad, D.-V. N. Vo, J. Iqbal and F. J. Stadler, *Appl. Catal., B*, 2021, **284**, 119808.

196 M. Zhu, Q. Liu, W. Chen, Y. Yin, L. Ge, H. Li and K. Wang, *ACS Appl. Mater. Interfaces*, 2017, **9**(44), 38832–38841.

197 W. Shi, C. Liu, M. Li, X. Lin, F. Guo and J. Shi, *J. Hazard. Mater.*, 2020, **389**, 121907.

198 X. Wang, Q. Lu, Y. Sun, K. Liu, J. Cui, C. Lu and H. Dai, *J. Environ. Chem. Eng.*, 2022, **10**(5), 108354.

199 N. Sedaghati, A. Habibi-Yangjeh, M. Pirhashemi and S. Vadivel, *J. Photochem. Photobiol., A*, 2019, **384**, 112066.

200 S. Zarezadeh, A. Habibi-Yangjeh, M. Mousavi and S. Ghosh, *J. Photochem. Photobiol., A*, 2020, **389**, 112247.

201 H. R. Kim, A. Razzaq, C. A. Grimes and S.-I. In, *J. CO₂ Util.*, 2017, **20**, 91–96.

202 W. Ali, H. Ullah, A. Zada, W. Muhammad, S. Ali, S. Shaheen, M. K. Alamgir, M. Z. Ansar, Z. U. Khan, H. Bilal and P.-S. Yap, *Sci. Total Environ.*, 2020, **746**, 141291.

203 W. Chen, S. Zhang, G. Wang, G. Huang, Z. Yu, Y. Li and L. Tang, *Nanomaterials*, 2021, **11**, 38.

204 Z. Ai, Y. Shao, B. Chang, B. Huang, Y. Wu and X. Hao, *Appl. Catal., B*, 2019, **242**, 202–208.

205 P. K. Prajapati, D. Garg, A. Malik, D. Kumar, V. Amoli and S. L. Jain, *J. Environ. Chem. Eng.*, 2022, **10**(4), 108147.

206 P. Basyach, P. K. Prajapati, S. S. Rohman, K. Sonowal, L. Kalita, A. Malik, A. K. Guha, S. L. Jain and L. Saikia, *ACS Appl. Mater. Interfaces*, 2023, **15**(1), 914–931.

207 D. Liu, L. Jiang, D. Chen, Z. Hao, B. Deng, Y. Sun, X. Liu, B. Jia, L. Chen and H. Liu, *ACS Catal.*, 2024, **14**(7), 5326–5343.

208 D. Majhi, K. Das, R. Bariki, S. Padhan, A. Mishra, R. Dhiman, P. Dash, B. Nayak and B. G. Mishra, *J. Mater. Chem. A*, 2020, **8**(41), 21729–21743.

209 Z.-J. Chen, H. Guo, H.-Y. Liu, C.-G. Niu, D.-W. Huang, Y.-Y. Yang, C. Liang, L. Li and J.-C. Li, *Chem. Eng. J.*, 2022, **438**, 135471.

210 B. Gao, Y. Pan and H. Yang, *Appl. Catal., B*, 2022, **315**, 121580.

211 M. Tayyab, Y. Liu, Z. Liu, L. Pan, Z. Xu, W. Yue, L. Zhou, J. Lei and J. Zhang, *J. Colloid Interface Sci.*, 2022, **628**, 500–512.

212 K. S. Novoselov, A. K. Geim, S. V. Morozov, D. Jiang, Y. Zhang, S. V. Dubonos, I. V. Grigorieva and A. A. Firsov, *Sci.*, 2004, **306**(5696), 666–669.

213 K. S. Novoselov, A. Mishchenko, A. Carvalho and A. H. Castro Neto, *Sci.*, 2016, **353**(6298), aac9439.

214 H. Yin, C. Yuan, H. Lv, X. Chen, K. Zhang and Y. Zhang, *Sep. Purif. Technol.*, 2022, **295**, 121294.

215 K. R. G. Lim, A. D. Handoko, S. K. Nemani, B. Wyatt, H. Y. Jiang, J. Tang, B. Anasori and Z. W. Seh, *ACS Nano*, 2020, **14**(9), 10834–10864.

216 H. Wang, F. Liu, W. Fu, Z. Fang, W. Zhou and Z. Liu, *Nanoscale*, 2014, **6**(21), 12250–12272.

217 C. Tan, P. Yu, Y. Hu, J. Chen, Y. Huang, Y. Cai, Z. Luo, B. Li, Q. Lu, L. Wang, Z. Liu and H. Zhang, *J. Am. Chem. Soc.*, 2015, **137**(32), 10430–10436.

218 I. Ahmad, S. Shukrullah, M. Y. Naz, M. Ahmad, E. Ahmed, Y. Liu, A. Hussain, S. Iqbal and S. Ullah, *Adv. Colloid Interface Sci.*, 2022, **304**, 102661.

219 H. Wang, X. Liu, P. Niu, S. Wang, J. Shi and L. Li, *Matter*, 2020, **2**(6), 1377–1413.

220 M. Xiong, J. Yan, B. Chai, G. Fan and G. Song, *J. Mater. Sci. Technol.*, 2020, **56**, 179–188.

221 X. Liu, Y. Liu, W. Zhang, Q. Zhong and X. Ma, *Mater. Sci. Semicon. Process.*, 2020, **105**, 104734.

222 Y. Guo, B. Chang, T. Wen, S. Zhang, M. Zeng, N. Hu, Y. Su, Z. Yang and B. Yang, *J. Colloid Interface Sci.*, 2020, **567**, 213–223.

223 J. Su, G. D. Li, X. H. Li and J. S. Chen, *Adv. Sci.*, 2019, **6**(7), 1801702.

224 X. Duan, C. Wang, J. C. Shaw, R. Cheng, Y. Chen, H. Li, X. Wu, Y. Tang, Q. Zhang, A. Pan, J. Jiang, R. Yu, Y. Huang and X. Duan, *Nat. Nanotechnol.*, 2014, **9**(12), 1024–1030.

225 S. Cheng, Z. Zuo and Y. Li, *Mater. Chem. Front.*, 2024, **8**(7), 1835–1843.

226 Y. Zhao, S. Zhang, R. Shi, G. I. N. Waterhouse, J. Tang and T. Zhang, *Mater. Today*, 2020, **34**, 78–91.

227 B. Tahir, M. Tahir and M. G. M. Nawawi, *J. CO₂ Util.*, 2020, **41**, 101270.

228 M. Antoniadou, M. K. Arfanis, I. Ibrahim and P. Falaras, *Water*, 2019, **11**(12), 2439.

229 W. Chen, M. Liu, X. Li and L. Mao, *Appl. Surf. Sci.*, 2020, **512**, 145782.

230 M. F. R. Samsudin, H. Ullah, R. Bashiri, N. M. Mohamed, S. Sufian and Y. H. Ng, *ACS Sustainable Chem. Eng.*, 2020, **8**(25), 9393–9403.

231 H. Sepahvand and S. Sharifnia, *Int. J. Hydrogen Energy*, 2019, **44**(42), 23658–23668.

232 J. Mao, B. Hong, J. Wei, J. Xu, Y. Han, H. Jin, D. Jin, X. Peng, J. Li, Y. Yang, J. Gong, H. Ge and X. Wang, *ChemistrySelect*, 2019, **4**(46), 13716–13723.

233 X. She, J. W. H. Xu, J. Zhong, Y. Wang, Y. Song, K. Nie, Y. Liu, Y. Yang, M. T. F. Rodrigues, R. Vajtai, J. Lou, D. Du, H. Li and P. M. Ajayan, *Adv. Energy Mater.*, 2017, **7**, 1700025.

234 P. John, K. Johari, N. Gnanasundaram, A. Appusamy and M. Thanabalan, *Environ. Technol. Innovation*, 2021, **22**, 101412.

235 Z. Han, X. Ning, Z. Yin, W. Zhen, G. Lu and B. Su, *Int. J. Hydrogen Energy*, 2024, **59**, 856–865.

© 2025 The Author(s). Published by the Royal Society of Chemistry

RSC Appl. Interfaces, 2025, **2**, 897–916 | 913

236 L. Jing, W.-J. Ong, R. Zhang, E. Pickwell-MacPherson and C. Y. Jimmy, *Catal. Today*, 2018, **315**, 103–109.

237 Y. Shang, H. Fan, Y. Sun and W. Wang, *Sustainable Energy Fuels*, 2022, **6**(16), 3729–3739.

238 S. Tao, L. Chenxi, B. Yupeng, F. Jun and L. Enzhou, *Acta Phys.-Chim. Sin.*, 2023, **39**(6), 2212009.

239 B. Wang, D. Chen, N. Li, Q. Xu, H. Li, J. He and J. Lu, *J. Colloid Interface Sci.*, 2020, **576**, 426–434.

240 Z. Zhang, J. Huang, Y. Fang, M. Zhang, K. Liu and B. Dong, *Adv. Mater.*, 2017, **29**(18), 1606688.

241 Y. Huang, F. Mei, J. Zhang, K. Dai and G. Dawson, *Acta Phys.-Chim. Sin.*, 2021, **0**(0), 2108028.

242 Q. Liu, X. He, J. Peng, X. Yu, H. Tang and J. Zhang, *Chin. J. Catal.*, 2021, **42**(9), 1478–1487.

243 Y. You, S. Wang, K. Xiao, T. Ma, Y. Zhang and H. Huang, *ACS Sustainable Chem. Eng.*, 2018, **6**(12), 16219–16227.

244 C. Ji, S.-N. Yin, S. Sun and S. Yang, *Appl. Surf. Sci.*, 2018, **434**, 1224–1231.

245 C. Liu, Y. Feng, Z. Han, Y. Sun, X. Wang, Q. Zhang and Z. Zou, *Chin. J. Catal.*, 2021, **42**(1), 164–174.

246 R.-T. Guo, X.-Y. Liu, H. Qin, Z.-Y. Wang, X. Shi, W.-G. Pan, Z.-G. Fu, J.-Y. Tang, P.-Y. Jia, Y.-F. Miao and J.-W. Gu, *Appl. Surf. Sci.*, 2020, **500**, 144059.

247 T. Yang, P. Deng, L. Wang, J. Hu, Q. Liu and H. Tang, *Chin. J. Struct. Chem.*, 2022, **41**(6), 2206023–2206030.

248 X. Gu, T. Chen, J. Lei, Y. Yang, X. Zheng, S. Zhang, Q. Zhu, X. Fu, S. Meng and S. Chen, *Chin. J. Catal.*, 2022, **43**(10), 2569–2580.

249 D. Gogoi, M. R. Das and N. Nath Ghosh, *Appl. Surf. Sci.*, 2023, **619**, 156753.

250 Z. Liang, L. Yunfeng, Z. Yongkang, Q. Liewei and X. Yan, *Acta Phys.-Chim. Sin.*, 2022, **38**(7), 2112027.

251 C. Liu, H. Dai, C. Tan, Q. Pan, F. Hu and X. Peng, *Appl. Catal., B*, 2022, **310**, 121326.

252 M. Alhaddad, R. M. Mohamed and M. H. H. Mahmoud, *ACS Omega*, 2021, **6**(12), 8717–8725.

253 J. Li, W. Cao, Y. Li, X. Xu, Y. Jiang and K. Lin, *ACS Appl. Energy Mater.*, 2022, **5**(8), 9463–9470.

254 X. Li, K. Xie, L. Song, M. Zhao and Z. Zhang, *ACS Appl. Mater. Interfaces*, 2017, **9**(29), 24577–24583.

255 R. Shen, J. Xie, X. Lu, X. Chen and X. Li, *ACS Sustainable Chem. Eng.*, 2018, **6**(3), 4026–4036.

256 Z. Jin, R. Hu, H. Wang, J. Hu and T. Ren, *Appl. Surf. Sci.*, 2019, **491**, 432–442.

257 W. Chen, Z.-C. He, G.-B. Huang, C.-L. Wu, W.-F. Chen and X.-H. Liu, *Chem. Eng. J.*, 2019, **359**, 244–253.

258 E. Sitara, H. Nasir, A. Mumtaz, M. F. Ehsan, M. Sohail, S. Iram, S. A. B. Bukhari, S. Ullah, T. Akhtar and A. Iqbal, *Int. J. Hydrogen Energy*, 2021, **46**(50), 25424–25435.

259 H. Sun and S.-J. Park, *Appl. Surf. Sci.*, 2020, **531**, 147325.

260 M. Ding, J. Zhou, H. Yang, R. Cao, S. Zhang, M. Shao and X. Xu, *Chin. Chem. Lett.*, 2020, **31**(1), 71–76.

261 D. Liu, D. Chen, N. Li, Q. Xu, H. Li, J. He and J. Lu, *Angew. Chem., Int. Ed.*, 2020, **59**(11), 4519–4524.

262 Q. Xu, B. Zhu, C. Jiang, B. Cheng and J. Yu, *Sol. RRL*, 2018, **2**(3), 1800006.

263 L. K. Putri, B.-J. Ng, W.-J. Ong, H. W. Lee, W. S. Chang and S.-P. Chai, *J. Mater. Chem. A*, 2018, **6**(7), 3181–3194.

264 L. Wang, Y. Li and P. Han, *Sci. Rep.*, 2021, **11**(1), 22950.

265 H. Dong, S. Hong, P. Zhang, S. Yu, Y. Wang, S. Yuan, H. Li, J. Sun, G. Chen and C. Li, *Chem. Eng. J.*, 2020, **395**, 125150.

266 P. Xia, B. Zhu, B. Cheng, J. Yu and J. Xu, *Chem. Eng.*, 2017, **6**(1), 965–973.

267 Z. Mo, H. Xu, Z. Chen, X. She, Y. Song, J. Lian, X. Zhu, P. Yan, Y. Lei, S. Yuan and H. Li, *Appl. Catal., B*, 2019, **241**, 452–460.

268 L. Chen, Y. Xu and B. Chen, *Appl. Catal., B*, 2019, **256**, 117848.

269 F. Guo, W. Shi, C. Zhu, H. Li and Z. Kang, *Appl. Catal., B*, 2018, **226**, 412–420.

270 B. Zhu, H. Tan, J. Fan, B. Cheng, J. Yu and W. Ho, *J. Materiomics*, 2021, **7**(5), 988–997.

271 S. Shi, M. Jia, M. Li, S. Zhou, Y. Zhao, J. Zhong, D. Dai and J. Qiu, *Colloids Surf., A*, 2023, **667**, 131259.

272 J. Jia, Y. Luo, H. Wu, Y. Wang, X. Jia, J. Wan, Y. Dang, G. Liu, H. Xie and Y. Zhang, *J. Colloid Interface Sci.*, 2024, **658**, 966–975.

273 S. Wang, P. He, L. Jia, M. He, T. Zhang, F. Dong, M. Liu, H. Liu, Y. Zhang, C. Li, J. Gao and L. Bian, *Appl. Catal., B*, 2019, **243**, 463–469.

274 M. Liu, S. Wei, W. Chen, L. Gao, X. Li, L. Mao and H. Dang, *J. Chin. Chem. Soc.*, 2020, **67**(2), 246–252.

275 R. Zahra, E. Pervaiz, M. M. Baig and O. Rabi, *Electrochim. Acta*, 2022, **418**, 140346.

276 D. T. N. Hoa, N. T. T. Tu, H. Q. A. Thinh, L. Van Thanh Son, L. V. T. Son, N. D. V. Quyen, L. L. Son, T. N. Tuyen, P. L. M. Thong, L. H. Diem and D. Q. Khieu, *J. Nanomater.*, 2023, **2023**(1), 9967890.

277 A. Alsalme, A. H. Galal, E. F. El-Sherbeny, A. Soltan, M. F. Abdel-Messih and M. A. Ahmed, *Diamond Relat. Mater.*, 2022, **122**, 108819.

278 T. Zhang, Q. Yang, H. Li, J. Zhong, J. Li and H. Yang, *Opt. Mater.*, 2022, **131**, 112649.

279 B. Zhang, X. Hu, E. Liu and J. Fan, *Chin. J. Catal.*, 2021, **42**(9), 1519–1529.

280 Y. Huo, J. Zhang, Z. Wang, K. Dai, C. Pan and C. Liang, *J. Colloid Interface Sci.*, 2021, **585**, 684–693.

281 B. Dai, Y. Li, J. Xu, C. Sun, S. Li and W. Zhao, *Appl. Surf. Sci.*, 2022, **592**, 153309.

282 H. Wang, R. Niu, J. Liu, S. Guo, Y. Yang, Z. Liu and J. Li, *Nano Res.*, 2022, **15**(8), 6987–6998.

283 T. Ni, H. Zhang, Z. Yang, L. Zhou, L. Pan, C. Li, Z. Yang and D. Liu, *J. Colloid Interface Sci.*, 2022, **625**, 466–478.

284 Q. Ding, X. Zou, J. Ke, Y. Dong, Y. Cui, G. Lu and H. Ma, *Renewable Energy*, 2023, **203**, 677–685.

285 K. Wang, X. Feng, Y. Shangguan, X. Wu and H. Chen, *Chin. J. Catal.*, 2022, **43**(2), 246–254.

286 Y. Zhen, C. Yang, H. Shen, W. Xue, C. Gu, J. Feng, Y. Zhang, F. Fu and Y. Liang, *Phys. Chem. Chem. Phys.*, 2020, **22**(45), 26278–26288.

287 A. Meng, S. Zhou, D. Wen, P. Han and Y. Su, *Chin. J. Catal.*, 2022, **43**(10), 2548–2557.

288 X. Lin, A. Kumar, G. Sharma, M. Naushad, G.-P. Alberto and F. J. Stadler, *J. Mol. Liq.*, 2022, **366**, 120147.

289 F. A. Qaraah, S. A. Mahyoub, A. Hezam, A. Qaraah, F. Xin and G. Xiu, *Appl. Catal., B*, 2022, **315**, 121585.

290 Z. Huang, J. Liu, S. Zong, X. Wang, K. Chen, L. Liu and Y. Fang, *J. Colloid Interface Sci.*, 2022, **606**(Pt 1), 848–859.

291 J. Fu, Q. Xu, J. Low, C. Jiang and J. Yu, *Appl. Catal., B*, 2019, **243**, 556–565.

292 D. Ren, W. Zhang, Y. Ding, R. Shen, Z. Jiang, X. Lu and X. Li, *Sol. RRL*, 2020, **4**(8), 1900423.

293 B. Liu, C. Bie, Y. Zhang, L. Wang, Y. Li and J. Yu, *Langmuir*, 2021, **37**(48), 14114–14124.

294 M. H. Barzegar, M. M. Sabzehmeidani, M. Ghaedi, V. M. Avargani, Z. Moradi, V. A. L. Roy and H. Heidari, *Chem. Eng. Res. Des.*, 2021, **174**, 307–318.

295 Y. Wang, Q. Wang, X. Zhan, F. Wang, M. Safdar and J. He, *Nanoscale*, 2013, **5**(18), 8326–8339.

296 G. Di Liberto, S. Tosoni and G. Pacchioni, *Adv. Funct. Mater.*, 2021, **31**(20), 2009472.

297 G. Di Liberto, S. Tosoni and G. Pacchioni, *J. Phys.: Condens. Matter*, 2019, **31**(43), 434001.

298 G. Di Liberto, A. Morales-Garcia and S. T. Bromley, *Nat. Commun.*, 2022, **13**(1), 6236.

299 G. Di Liberto, S. Tosoni and G. Pacchioni, *J. Phys.: Condens. Matter*, 2021, **33**(7), 075001.

300 Y. Chang, J. R. Yates and C. E. Patrick, *ACS Omega*, 2023, **8**(22), 20138–20147.

301 X. Hao, Q. Ma, X. Zhang, J. Wang, D. Yin, S. Ma and B. Xu, *J. Appl. Phys.*, 2024, **136**(6), 064303.

302 X. Liu, J. Chen, H. Yin, L. Bai, C. Yao, H. Li, H. Yin and Y. Wang, *Mater. Res. Lett.*, 2019, **7**(6), 232–238.

303 Y. Qi, M. A. Sadi, D. Hu, M. Zheng, Z. Wu, Y. Jiang and Y. P. Chen, *Adv. Mater.*, 2023, **35**(12), e2205714.

304 P. A. Vermeulen, J. Mulder, J. Momand and B. J. Kooi, *Nanoscale*, 2018, **10**(3), 1474–1480.

305 T. Huang, W. Wei, X. Chen and N. Dai, *Ann. Phys.*, 2019, **531**(4), 1800465.

306 J. Yang, X. Li, Y. Yang and R. Dou, *J. Phys. Chem. Lett.*, 2025, **16**(11), 2731–2741.

307 Q. Li, C. Pan, J. Wang, L.-L. Wang and X. Zhu, *Appl. Surf. Sci.*, 2022, **605**, 154720.

308 G. Di Liberto, L. A. Cipriano, S. Tosoni and G. Pacchioni, *Chem*, 2021, **27**(53), 13306–13317.

309 R. Tao, X. Li, X. Li, C. Shao and Y. Liu, *Nanoscale*, 2020, **12**(15), 8320–8329.

310 N. D. Lam, H. Van Thanh, T. D. Thien and T. Nguyen-Tran, *Mater. Trans.*, 2023, **64**(2), 578–585.

311 J.-M. Delgado-Sanchez, I. Lillo-Bravo, J. A. López-Álvarez and E. Pérez-Aparicio, *Sol. RRL*, 2022, **6**(12), 2200818.

312 M. A. Hanif, J. Akter, Y. S. Kim, H. G. Kim, J. R. Hahn and L. K. Kwac, *Catal.*, 2022, **12**(2), 151.

313 C. G. Van de Walle and R. M. Martin, *Phys. Rev. B: Condens. Matter*, 1987, **35**(15), 8154–8165.

314 G. Di Liberto, S. Tosoni and G. Pacchioni, *Phys. Chem. Chem. Phys.*, 2019, **21**(38), 21497–21505.

315 S.-H. Wei and A. Zunger, *Appl. Phys. Lett.*, 1998, **72**(16), 2011–2013.

316 S.-H. Wei and A. Zunger, *J. Appl. Phys.*, 1995, **78**(6), 3846–3856.

317 J. C. Conesa, *Nanomaterials*, 2021, **11**(6), 1581.

318 D. O. Scanlon, C. W. Dunnill, J. Buckeridge, S. A. Shevlin, A. J. Logsdail, S. M. Woodley, C. R. Catlow, M. J. Powell, R. G. Palgrave, I. P. Parkin, G. W. Watson, T. W. Keal, P. Sherwood, A. Walsh and A. A. Sokol, *Nat. Mater.*, 2013, **12**(9), 798–801.

319 G. Di Liberto, S. Tosoni, F. Illas and G. Pacchioni, *J. Chem. Phys.*, 2020, **152**(18), 184704.

320 R. W. Grant, E. A. Kraut, S. P. Kowalczyk and J. R. Waldrop, *J. Vac. Sci. Technol., B: Microelectron. Process. Phenom.*, 1983, **1**(2), 320–327.

321 J. R. Waldrop, S. P. Kowalczyk, R. W. Grant, E. A. Kraut and D. L. Miller, *J. Vac. Sci. Technol.*, 1981, **19**, 573–575.

322 I. E. L. Stephens, A. S. Bondarenko, L. Bech and I. Chorkendorff, *ChemCatChem*, 2012, **4**(3), 341–349.

323 E. A. Kraut, R. W. Grant, J. R. Waldrop and S. P. Kowalczyk, *Phys. Rev. B: Condens. Matter Mater. Phys.*, 1983, **28**(4), 1965–1977.

324 G. Di Liberto, S. Tosoni and G. Pacchioni, *ChemCatChem*, 2020, **12**(7), 2097–2105.

325 N. Pueyo Bellafont, F. Vines, W. Hieringer and F. Illas, *J. Comput. Chem.*, 2017, **38**(8), 518–522.

326 F. Vines, C. Sousa and F. Illas, *Phys. Chem. Chem. Phys.*, 2018, **20**(13), 8403–8410.

327 I. Grigioni, G. Di Liberto, M. V. Dozzi, S. Tosoni, G. Pacchioni and E. Selli, *ACS Appl. Energy Mater.*, 2021, **4**(8), 8421–8431.

328 P. Lv, F. Duan, J. Sheng, S. Lu, H. Zhu, M. Du and M. Chen, *Appl. Organomet. Chem.*, 2020, **35**(3), e6124.

329 S. Kumar, A. Kumar, A. Kumar, R. Balaji and V. Krishnan, *ChemistrySelect*, 2018, **3**(6), 1919–1932.

330 Y. Lu, Z. Zhuang, L. Li, F.-F. Chen, P. Wei and Y. Yu, *J. Mater. Chem. A*, 2025, **13**, 4718–4745.

331 Y. Guo, W. Shi and Y. Zhu, *EcoMat*, 2019, **1**(1), e12007.

332 T. Lv, J. Li, N. Arif, L. Qi, J. Lu, Z. Ye and Y.-J. Zeng, *Matter*, 2022, **5**(9), 2685–2721.

333 F. Chen, H. Huang, L. Guo, Y. Zhang and T. Ma, *Angew. Chem., Int. Ed.*, 2019, **58**(30), 10061–10073.

334 X. Yue, J. Fan and Q. Xiang, *Adv. Funct. Mater.*, 2021, **32**(12), 2110258.

335 Z. Lou, P. Wang, B. Huang, Y. Dai, X. Qin, X. Zhang, Z. Wang and Y. Liu, *ChemPhotoChem.*, 2017, **1**(5), 136–147.

336 Z. Wang, B. Cheng, L. Zhang, J. Yu and H. Tan, *Sol. RRL*, 2021, **6**(1), 2100587.

337 W. Lou, G. Liu, X. Ma, C. Yang, L. Feng, Y. Liu and X. Gao, *J. Mater. Chem. A*, 2025, **13**(6), 4356–4366.

338 L. Sun, W. Wang, C. Zhang, M. Cheng, Y. Zhou, Y. Yang, H. Luo, D. Qin, C. Huang and Z. Ouyang, *Chem. Eng. J.*, 2022, **446**, 137027.

339 W. Ouyang, F. Teng and X. Fang, *Adv. Funct. Mater.*, 2018, **28**(16), 1707178.

© 2025 The Author(s). Published by the Royal Society of Chemistry

RSC Appl. Interfaces, 2025, **2**, 897–916 | **915**

340 Y. Zhong, *Front. Chem.*, 2023, **11**, 1278370.

341 R. Long, W.-H. Fang and O. V. Prezhdo, *J. Phys. Chem. C*, 2017, **121**(7), 3797–3806.

342 Y. Guo, Y. Xue, X. Li, C. Li, H. Song, Y. Niu, H. Liu, X. Mai, J. Zhang and Z. Guo, *Nanomaterials*, 2019, **9**(7), 966.

343 K. Zhang, M. Fujitsuka, Y. Du and T. Majima, *ACS Appl. Mater. Interfaces*, 2018, **10**(24), 20458–20466.

344 J. Hu, D. Chen, Z. Mo, N. Li, Q. Xu, H. Li, J. He, H. Xu and J. Lu, *Angew. Chem., Int. Ed.*, 2019, **58**(7), 2073–2077.

345 J. Shi, L. Mao, C. Cai, G. Li, C. Cheng, B. Zheng, Y. Hu, Z. Huang, X. Hu and G. Żyła, *Catal. Sci. Technol.*, 2020, **10**(17), 5896–5902.

346 X. Tao, Y. Gao, S. Wang, X. Wang, Y. Liu, Y. Zhao, F. Fan, M. Dupuis, R. Li and C. Li, *Adv. Energy Mater.*, 2019, **9**(13), 1803951.